Journal of Statistical Physics, Vol. 1, No. 1, 1969

Limiting Polytope Geometry for Rigid Rods, Disks, and Spheres

Frank H. Stillinger, Jr.,[1] and Zevi W. Salsburg[2]

Received February 13, 1969

The available configuration space for finite systems of rigid particles separates into equivalent disconnected regions if those systems are highly compressed. This paper presents a study of the geometric properties of the limiting high-compression regions (polytopes) for rods, disks, and spheres. The molecular distribution functions represent cross sections through the convex polytopes, and for that reason they are obliged to exhibit single-peak behavior by the Brünn–Minkowski inequality. We demonstrate that increasing system dimensionality implies tendency toward nearest-neighbor particle-pair localization away from contact. The relation between the generalized Euler theorem for the limiting polytopes and cooperative "jamming" of groups of particles is explored. A connection is obtained between the moments of inertia of the polytopes (regarded as solid homogeneous bodies) and crystal elastic properties. Finally, we provide a list of unsolved problems in this geometrical many-body theory.

KEY WORDS: Rigid spheres; Rigid disks; Rigid rods; Elasticity; High pressure; Polytopes; Convexity; Crystal anharmonicity; Pair correlation functions; Multidimensional geometry; Crystalline order; Crystal defects.

1. INTRODUCTION

The hard-sphere system has been one of the most important and convenient models available to the theoretician during the development of modern statistical mechanics. Its attractiveness is largely due to easy visualization of energetically allowed particle configurations. Also, the relevant mathematical analysis, while generally far from trivial, is still relatively simpler than corresponding analysis for other molecular models which specify "softer" collisions.

The major portion of past theoretical effort on the hard-sphere model has been devoted to the fluid state.[1] However, this model has the fascinating virtue of crystal-

[1] Bell Telephone Laboratories, Inc., Murray Hill, New Jersey 07974.
[2] Department of Chemistry, Rice University, Houston, Texas 77001.

lizing under sufficient compression, and probably the resulting solid phase has a far richer variety of interesting phenomena to study than the fluid. The hard-sphere crystal also commands special attention because of its extreme anharmonicity; comparison of its properties with those of the conventional harmonic crystal models should illuminate the role of varying anharmonicity in real solids.

This paper will survey one aspect of the classical hard-sphere solid, namely, its behavior in the high-compression limit. In doing so, we shall actually consider the set of related "sphere" systems of varying dimensionality ν, such that $\nu = 1, 2, 3,...$, correspond respectively to rigid rods on a line, disks in a plane, spheres in 3-space,... . Our unifying point of view for this sequence will be that of the geometer studying the properties of the allowed region in the multidimensional configuration space. The high-compression limit provides the advantage that this allowed region reduces to a set of identical disjoint convex polytopes (multidimensional "polyhedra") for which a substantial body of deep geometrical theory is available.

A further advantage of the high-compression limit for $\nu > 1$ is the freedom to freeze various defects into the crystal. Simple vacancies and dislocations are immobile in this limit, and may be placed at will. It then becomes possible to study their effect on free energy and elastic properties, and to make comparisons with continuum defect theory.[2]

The hard-sphere system and its lower-dimensional analogs have been favorite subjects for electronic computer simulation of many-body problems. We are therefore fortunate that increasing attention is being devoted to computation of their solid-state properties.[3,4] The expanding area of agreement between these computer studies and pure theory of the type to follow in this paper we believe is valuable not only by lending added credence to both approaches, but also by stimulating further activity and interest in these specialized solid-state studies.

Attention in this paper will be restricted entirely to equilibrium properties of the high-compression crystals. Nevertheless, we view the geometric considerations below as a necessary preliminary to fabrication of a general kinetic theory of the rigid-sphere crystal. In particular, this task would require construction of at least approximate eigenfunctions for the Liouville operator inside the configuration space polytope which is the primary object of attention in this paper.

Unfortunately we are unable to eliminate a basic logical weakness in the high-compression theory. This is associated with the fact that as the number of particles N in the system (when $\nu > 1$) tends to infinity, one is strictly confined to a smaller and smaller density interval around close packing.[5] Just below the close-packed density, for sufficiently large N, the normally small polytope face curvatures conspire in certain special directions to produce thin "tubes" or "filaments" which actually connect the polytopes. However, there is no reason to believe that these narrow connections have any weight in determining the usual system intensive properties. Therefore we shall formally disregard this feature in anticipation of an ultimate demonstration of the commutability of the $N \to \infty$ and the high-compression limits for the stable crystal modifications.

2. ELEMENTARY FEATURES OF LIMITING POLYTOPES

2.1. Definition of the Polytopes

To the best of our knowledge, the previously cited paper by Salsburg and Wood[5] is the only publication which has explicitly considered the limiting high-compression geometrical structure of available configuration space for hard spheres. We now retrace some of that earlier work for completeness, as well as to incorporate some modifications that are desirable for our present purposes.

Let N rigid ν-spheres be contained in a region Ω of Euclidean ν-space. The canonical partition function gives the system's Helmholtz free energy F_N:

$$\exp(-\beta F_N) = (\lambda^{\nu N} N!)^{-1} \int_\Omega d\mathbf{r}_1 \cdots \int_\Omega d\mathbf{r}_N \exp\left\{-\beta \sum_{i<j=1}^{N} \varphi(ij)\right\} \tag{1}$$
$$\beta = (k_B T)^{-1}, \qquad \lambda = h(2\pi m k_B T)^{-1/2}$$

Here the ν-vector $\mathbf{r}_i$ locates the center of sphere i. The hard-sphere pair potential φ is infinite for distances less than diameter a, but zero otherwise, so that the integrand in (1) may be expressed simply as a product of unit step functions:

$$\exp(-\beta F_N) = (\lambda^{\nu N} N!)^{-1} \int_\Omega d\mathbf{r}_1 \cdots \int_\Omega d\mathbf{r}_N \sum_{i<j=1}^{N} U(|\,\mathbf{r}_i - \mathbf{r}_j\,| - a) \tag{2}$$
$$U(x) = 0, \qquad x < 0$$
$$= 1, \qquad x \geqslant 0$$

It will be convenient to suppose that the system is subject to periodic boundary conditions. Compressions and decompressions then will be produced by changing the size of the periodicity cell Ω *at constant shape*. Furthermore this basic shape will be selected to conform to the global close-packing of the N spheres (and their periodic images) throughout all of ν-space. For the moment we shall suppose that integer N allows packing into a perfect crystal, i.e., without vacancies or other defects. Figure 1 illustrates cell Ω and the perfect packing for a set of $N = 16$ rigid disks in the plane; the figure also illustrates the freedom, aside from translation, that exists for $\nu \geqslant 2$ in selection of Ω according to which particles are considered basic, and which ones merely images.

Although particles are held tightly against one another when Ω has that minimum size Ω_0 producing close packing, the system as a whole may still freely translate as a result of the boundary conditions. Such translations allow any one particle to be moved from its original position to the position initially occupied by any of the other particles. If Ω's boundaries had been hard, impenetrable walls, there would have been $N!$ independent ways of placing the particles in the packed state. But with periodic boundary conditions, there are only

$$N!/N = (N-1)! \tag{3}$$

independent ways that cannot be interconverted without system decompression.

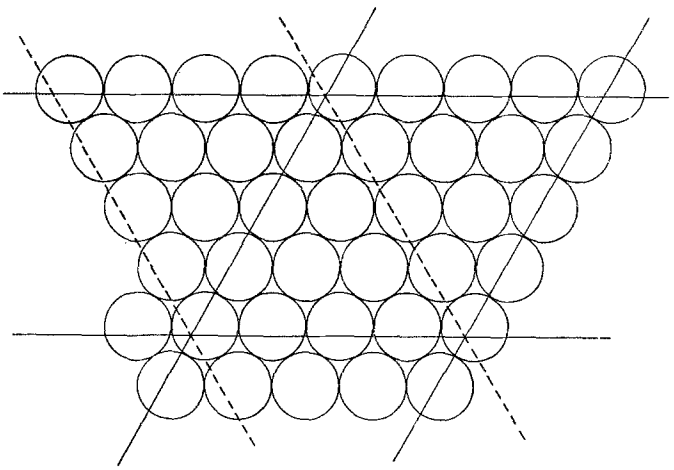

Fig. 1. Periodicity cell Ω for $N = 16$ rigid disks in the plane. The boundary of Ω is indicated by solid lines. An alternative choice (but dynamically identical) is shown by the dashed, rather than solid, oblique lines.

The full configuration space for the system of N ν-spheres is the (νN)-dimensional region generated by the direct product

$$\Omega^* = \Omega_1 \times \Omega_2 \times \cdots \times \Omega_N \tag{4}$$

of Ω-cells for the individual particles as subscripted. At close packing, the only points of Ω^* that are accessible to the system (that is, have no sphere overlaps) will be the $(N-1)!$ separate domains, each of dimensionality ν, which correspond to the distinct, freely translating crystals. However, when Ω increases a small finite amount from Ω_0, the spheres are free to move slightly relative to each other, and the accessible regions become narrow (νN)-dimensional hyperprisms. The lateral boundary of each hyperprism consists of the set of hypersurfaces for possible nearest-neighbor sphere contacts in the given crystal arrangement. From Eq. (2) we see that the analytic representation of these hypersurfaces is simply

$$| \mathbf{r}_i - \mathbf{r}_j | = a \tag{5}$$

If z_ν stands for the number of nearest neighbors in the ν-sphere crystal, then there will be $\frac{1}{2}z_\nu N$ hypersurfaces (5) bounding the hyperprism (if the crystal is more than one particle wide in each direction).

One technical point deserves attention at this stage. Under translation of the crystal, the center-of-mass vector

$$\mathbf{R} = (\mathbf{r}_1 + \mathbf{r}_2 + \cdots + \mathbf{r}_N)/N \tag{6}$$

undergoes frequent jumps, as spheres cross Ω's boundaries. As they do, the corresponding $\mathbf{r}_j$ jump to an opposite Ω boundary, and $\mathbf{R}$ is affected accordingly. Each of

the $(N-1)!$ hyperprisms therefore actually occurs in N separate pieces inside Ω^*, but it is in the nature of the periodic boundary conditions that these N pieces could be reassembled by simple translations into the whole hyperprism. An alternative but equivalent statement is that in the full (νN)-dimensional configuration space filled by Ω^* and its periodic images, $N!$ infinitely long hyperprisms pierce Ω^*.

In order to give a concrete illustration of the preceding we have presented the three-dimensional configuration space for three rigid rods on a line ($\nu = 1$, $N = 3$) in Fig. 2. In this case there are three possible neighbor contacts of type (5) for the two possible "crystals," or translatable rod orderings. Indeed one sees that the prismatic accessible regions have three lateral faces each, and cross sections in the shape of equilateral triangles. In the close-packed limit, it is clear that these hyperprisms shrink onto their axes, to leave merely a set of parallel lines.

The axial length of each prism, properly assembled, for the example in Fig. 2 is $3^{1/2}\Omega$. For more general ν and N, the hyperprism axial measure can be computed to be $N^{\nu/2}\Omega$. [The computation is initiated by configuration-space coordinate rotation as described by Eq. (124) below.] Then if $S_N^{(\nu)}(\Omega)$ is the $[\nu(N-1)]$-dimensional cross-sectional measure of the hyperprism, the partition function (2) may be expressed thus:

$$\exp(-\beta F_N) = N^{(\nu/2)-1}\Omega S_N^{(\nu)}(\Omega)/\lambda^{\nu N} \tag{7}$$

Owing to the fact that $S_N^{(\nu)}(\Omega)$ shrinks to zero size as Ω decreases to Ω_0, it is convenient to transform from the original particle coordinates $\mathbf{r}_1, \ldots, \mathbf{r}_N$ to a reduced set of vectors $\mathbf{t}_1, \ldots, \mathbf{t}_N$ in terms of which the $\Omega \to \Omega_0$ limiting cross section remains finite. First, for given $\Omega \geqslant \Omega_0$ and a specific ordering of spheres in the crystal, let the

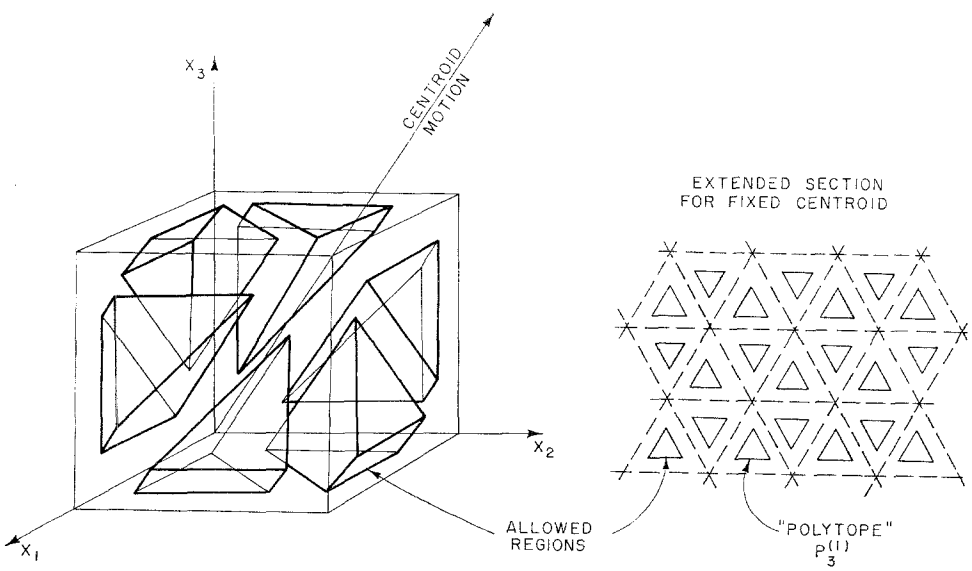

Fig. 2. Configuration space for three rigid rods on a line, subject to periodic boundary conditions. The unit cube shown should be imagined periodically replicated so as to fill space entirely. The section shown is then taken perpendicular to the threefold "centroid motion" axis.

center-of-mass position $\mathbf{R}$ be held fixed. Furthermore we shall denote by $\mathbf{r}_1^{(0)},\ldots,\mathbf{r}_N^{(0)}$ the regular lattice positions for the crystal that would be obtained by homogeneous expansion of the close-packed crystal from Ω_0 to Ω. The conditions specifying that the system lie in an accessible region of configuration space are, for all neighbor pairs i, j,

$$\begin{gathered} |\, \mathbf{r}_{ij}^{(0)} + \delta\mathbf{r}_j - \delta\mathbf{r}_i \,| - a \geqslant 0 \\ \mathbf{r}_{ij}^{(0)} = \mathbf{r}_j^{(0)} - \mathbf{r}_i^{(0)}, \qquad \delta\mathbf{r}_i = \mathbf{r}_i - \mathbf{r}_i^{(0)} \end{gathered} \tag{8}$$

When Ω is very close to Ω_0 it is obvious that the displacements $\delta\mathbf{r}_i$ of any particle from its nominal lattice position $\mathbf{r}_i^{(0)}$ will be small; in fact, they should be roughly of the order of the length of free travel in the homogeneously expanded crystal. Thus we are justified in expanding the left member of Eq. (8) and retaining only linear terms in the deviations:

$$\begin{gathered} [\mathbf{w}_{ij} \cdot (\mathbf{r}_{ij}^{(0)} + \delta\mathbf{r}_j - \delta\mathbf{r}_i)] - a \geqslant 0 \\ \mathbf{w}_{ij} = \mathbf{r}_{ij}^{(0)}/|\, \mathbf{r}_{ij}^{(0)} \,| \end{gathered} \tag{9}$$

Since we have

$$\Omega/\Omega_0 = (|\, \mathbf{r}_{ij}^{(0)} \,|/a)^\nu \tag{10}$$

the conditions (9) are equivalent in the high-compression limit to

$$1 + \mathbf{w}_{ij} \cdot (\mathbf{t}_j - \mathbf{t}_i) \geqslant 0 \tag{11}$$

where the reduced displacements are

$$\mathbf{t}_i = \{\nu/a[(\Omega/\Omega_0) - 1]\}\, \delta\mathbf{r}_i \tag{12}$$

The set of linear inequalities in (11) defines a polytope $P_N^{(\nu)}$ in the $[\nu(N-1)]$-dimensional subspace for fixed system center of mass.[6] This polytope is formed from the tangent hyperplanes[5] to the hypercylindrical surfaces (5) which actually bound the true cross section $S_N^{(\nu)}(\Omega)$. In the close-packed limit the curvature of $S_N^{(\nu)}$'s boundaries becomes less and less important; in other words

$$\lim_{\Omega \to \Omega_0} \frac{\{(a/\nu)(\Omega/\Omega_0 - 1)\}^{\nu(N-1)}\, P_N^{(\nu)}}{S_N^{(\nu)}(\Omega)} = 1 \tag{13}$$

From Eq. (7) we see that the high-compression free energy has the following behavior:

$$-\beta F_N \sim \ln \left\{ \frac{N^{(\nu/2)-1}\Omega}{\lambda^{\nu N}} \left[\frac{a}{\nu} \left(\frac{\Omega}{\Omega_0} - 1 \right) \right]^{\nu(N-1)} P_N^{(\nu)} \right\} \tag{14}$$

[There should be no confusion in the fact that we use symbol $P_N^{(\nu)}$ both for the polytope *and* its numerical content.]

Polytope $P_N^{(\nu)}$ is bounded by $\frac{1}{2}z_\nu N$ faces, each with dimensionality $\nu(N-1) - 1$. We see from (11) that these faces are analytically specified by the linear relations

$$1 + \mathbf{w}_{ij} \cdot (\mathbf{t}_j - \mathbf{t}_i) = 0 \tag{15}$$

for all the crystal's nearest-neighbor pairs (i, j), subject to the restraint

$$\sum_{i=1}^{N} \mathbf{t}_i = 0 \tag{16}$$

so as to remain in the fixed center-of-mass space. It is worth noting that the $P_N^{(1)}$ for N rigid rods are examples of simplexes,[7] since they are bounded by the minimum possible number N of faces that can enclose a finite region in $(N-1)$-dimensional space.

When the crystal is wider than two particles in any direction within Ω, we may state that all pairs of faces of $P_N^{(\nu)}$ intersect. That this is so follows from the fact that any two nearest-neighbor pairs of particles (whether sharing a particle or not) may simultaneously be in contact.

The further geometric properties of the polytopes $P_N^{(\nu)}$ are the major object of interest in the remainder of this paper.

2.2. Symmetry Properties

Perhaps the most obvious questions to ask about the $P_N^{(\nu)}$ concern their symmetries. First note that the symmetrical cells Ω (such as shown in Fig. 1) that are required by periodicity render any particle displacement $\mathbf{t}_i$ (system center of mass fixed, of course) just as likely as its negative, $-\mathbf{t}_i$. Thus the polytope centroid is located precisely at

$$\mathbf{t}_1 = \mathbf{t}_2 = \cdots = \mathbf{t}_N = 0 \tag{17}$$

It is then easy to see that this centroid will *not* be a center of inversion symmetry for $P_N^{(\nu)}$, for if it were any set of displacements $\mathbf{t}_1, \ldots, \mathbf{t}_N$ that correspond to a point on $P_N^{(\nu)}$'s surface (that is, contact between one or more particle pairs) would have a corresponding point $-\mathbf{t}_1, \ldots, -\mathbf{t}_N$ also on $P_N^{(\nu)}$'s surface. As Fig. 3 illustrates, however, it is a trivial matter to find a set of displacements whose negatives lead to particle overlap, and therefore correspond to a point *outside* $P_N^{(\nu)}$.

Nevertheless certain $P_N^{(\nu)}$ symmetries can be obtained if the inversion operation is combined with suitable reflection operations corresponding to permutation of the $\mathbf{t}_j$. In particular, if change in sign of all $\mathbf{t}_j$ is followed by their reassignment to particles directly across the center of ν-space cell Ω, the new point in configuration space again lies on the boundary of $P_N^{(\nu)}$. This is particularly evident in the example shown in Fig. 3,

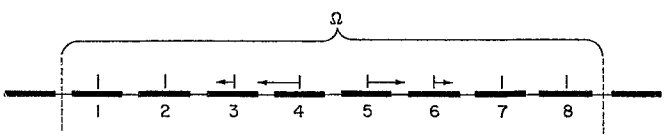

Fig. 3. Displacements (arrows) for eight rigid rods on a line. Since the four nonvanishing displacements lead to contacts (2,3), (3,4), (5,6), and (6,7), the corresponding configuration-space point lies in polytope $P_8^{(1)}$'s surface. However, the negatives of these displacements produce overlap between rods 4 and 5, and correspond to a point exterior to $P_8^{(1)}$. Clearly, similar displacement sets can be found for rigid disks or spheres.

where the combination of operations ends up replacing original rod displacement $\mathbf{t}_j$ by $-\mathbf{t}_{9-j}$ $(1 \leqslant j \leqslant 8)$.

For rigid rods, rigid disks, and rigid spheres stacked in a face-centered cubic crystal, all nearest-neighbor pairs of particles will be equivalent to one another. [Here we assume that when $\nu = 2$ the cell Ω is a rhombus, and when $\nu = 3$ it is an equilateral rhombohedron, so that the crystal has equal lengths in each direction of periodicity.] The $\frac{1}{2}z_\nu N$ faces of $P_N^{(\nu)}$ then are identical to one another in shape and size and so are superposable by translations and proper rotations. However, this does not mean that the $P_N^{(\nu)}$ are completely regular, for although these faces are each bounded $(N \geqslant 3^\nu)$ by

$$\frac{1}{2!}(\tfrac{1}{2}z_\nu N)(\tfrac{1}{2}z_\nu N - 1) \tag{18}$$

"edges" of dimensionality $\nu(N-1) - 2$ (one "edge" for each pair of contact pairs), these "edges" are not all of the same "length"; indeed their content measures relative probability for the double-contact coincidence, and this probability surely depends on how close the two pairs are to one another, as well as the angle between them.

The polytope $P_N^{(3)}$ for N rigid spheres placed in a hexagonally-close-packed crystal is necessarily less symmetrical than that for the face-centered crystal. Not all nearest-neighbor pairs are equivalent in h.c.p.; some are perpendicular to the hexagonal c axis, while others are obliquely inclined to it. It has previously been pointed out[8] that the inherently different polytope geometries for h.c.p. and f.c.c. crystals can lead to a difference in free energy for the two, with the former apparently the more stable thermodynamically.

Polytope symmetries can also be reduced for $\nu > 1$ by inclusion of vacancies in the compressed crystal. A crystal consisting of N particles and N_m nonneighboring monovacancies will again generate a $[\nu(N-1)]$-dimensional polytope, but it will now possess only $\frac{1}{2}z_\nu N - z_\nu N_m$ faces. Furthermore, these faces will fail to be equivalent to one another, since their corresponding particle pairs in the crystal can be variously arranged relative to the vacancies that are immobilized by the high compression. In a similar way, dislocations in three-dimensional sphere crystals will induce polytope symmetry lowering.

2.3. Polytope Face Arrangement

In order to facilitate discussion of polytope geometry, it is convenient to trace the movement of the system point in the full configuration space as small sets of particles move about. Thus to every ν-dimensional displacement vector $\mathbf{t}_i$ we assign a corresponding νN-dimensional vector $\mathbf{t}_i{}^*$, all of whose components are zero except in the i-particle subspace, where it has the same components as $\mathbf{t}_i$. The usual vector operations (such as scalar products, and length measure) on these multidimensional vectors and their sums are obvious generalizations of the more usual one-, two-, and three-dimensional versions.

We may easily identify the shortest path from the polytope center to any face, say that for neighbors i and j. This path corresponds to the symmetric movement of i and j directly toward one another along their line of centers, starting of course from

the perfect-crystal arrangement, until they just touch. From Eq. (15) we see that the requisite configuration-space vector for this process must be

$$\mathbf{t}_{ij}^{*} = \mathbf{t}_{i}^{*} + \mathbf{t}_{j}^{*} \tag{19}$$

formed from the ν-space vectors

$$\begin{aligned} \mathbf{t}_i &= \tfrac{1}{2}\mathbf{w}_{ij} \\ \mathbf{t}_j &= -\tfrac{1}{2}\mathbf{w}_{ij} \end{aligned} \tag{20}$$

Since $\mathbf{w}_{ij}$ is a unit vector, the magnitude of $\mathbf{t}_{ij}^{*}$, the distance from the polytope center to any face, must be

$$|\,\mathbf{t}_{ij}^{*}\,| = (|\,\mathbf{t}_i\,|^2 + |\,\mathbf{t}_j\,|^2)^{1/2} = 2^{-1/2} \tag{21}$$

It is simple to verify that $\mathbf{t}_{ij}^{*}$ is parallel to any outward normal to the (i, j) face, by virtue of being perpendicular to all vectors lying in the face and starting at the $\mathbf{t}_{ij}^{*}$ end point; these latter vectors correspond to further motions of any crystal particles (center of mass still fixed for the system) so long as the (i, j) contact is maintained. However, it is not true that $\mathbf{t}_{ij}^{*}$ touches face (i, j) at its centroid, since we should expect an *average* displacement of particles near i and j from their nominal lattice positions, when i and j are in contact, in the crystal's complete equilibrium distribution.

We can now find the angle between any two polytope faces, that is, the angle between their outward normal vectors. If the two faces are (i, j) and (k, l) contact faces, involving four distinct particles in the crystal, one has

$$\mathbf{t}_{ij}^{*} \cdot \mathbf{t}_{kl}^{*} = 0 \tag{22}$$

because there are no corresponding components of both vectors that are both simultaneously nonzero. Therefore pairs of faces of this type (the overwhelming majority for large N) are perpendicular. However if the two faces chosen involve a shared particle j, say faces (i, j) and (j, k), the scalar product analogous to (22) will have a nonvanishing contribution from the j-particle subspace. The angle θ between the faces is found to satisfy

$$\begin{aligned} \cos\theta &= \frac{\mathbf{t}_{ij}^{*} \cdot \mathbf{t}_{jk}^{*}}{|\,\mathbf{t}_{ij}^{*}\,|\,|\,\mathbf{t}_{jk}^{*}\,|} \\ &= -\tfrac{1}{2}\mathbf{w}_{ij} \cdot \mathbf{w}_{jk} \end{aligned} \tag{23}$$

For rigid rods only one type of triplet is possible and the angle between the faces is

$$\theta = \arccos(-\tfrac{1}{2}) = \tfrac{2}{3}\pi \tag{24}$$

Such linear triplets of course also occur in rigid disk and sphere crystals, and (24) also applies to them. But these $\nu > 1$ models have "bent" triplets as well, and the corresponding angles θ are smaller than $\frac{2}{3}\pi$, in some cases less than the very common $\frac{1}{2}\pi$. In any event, no pair of faces will be parallel, as already acknowledged by Eq. (18) (but note the requirement on N preceding that equation).

The end points of the vectors $\mathbf{t}_{ij}^{*}$ in the polytope faces are points which we may designate by O_{ij}. Each of these $\frac{1}{2}z_\nu N$ points lies on the inscribed hypersphere (with radius $r_{in} = 2^{-1/2}$) surrounding the polytope's center O. Because we now have an explicit vector representation of the O_{ij} relative to O, we may readily find the distance between the points O_{ij}. The results are the following:

(a) If points O_{ij} and O_{kl} belong to faces whose contact pairs involve four distinct particles, the distance is 1.

(b) If the points are O_{ij} and O_{jk}, with particle j common to both faces' contact pairs, the distance is $(1 + \frac{1}{2}\mathbf{w}_{ij} \cdot \mathbf{w}_{jk})^{1/2}$.

The minimum distance between face points O_{ij} is therefore 1 for $\nu = 1$, and occurs for pairs of faces that do not involve a common particle. However, when $\nu \geqslant 2$, the minimum distance is $\frac{1}{2}\sqrt{3}$, and is attained for two contact-pair faces which do have a common particle, with the relevant particle triplet in the "most bent" configuration: an equilateral triangle of particles. In all cases the distance between any two points O_{ij} exceeds the common distance of these points from the polytope center O.

On account of this last observation, it is possible to place $\frac{1}{2}z_\nu N$ nonoverlapping hyperspheres identical in size with the inscribed hypersphere simultaneously in exterior contact with that inscribed hypersphere at the points O_{ij}. Since it is known[9] that for large dimensionality n the maximum number of such nonoverlapping tangent hyperspheres varies essentially as $\exp(\alpha n)$, $\alpha > 0$, it is clear that as $N \to \infty$ our carefully placed $\frac{1}{2}z_\nu N$ hyperspheres are very sparsely distributed. The polytope faces are mutually tangent to the central inscribed hypersphere and the corresponding contact hypersphere. The sparseness of the distribution of these latter implies that these faces do not stay always close to the surface of the inscribed hypersphere. This last feature is reflected in the fact that the radius of the polytope's *circumscribed* hypersphere (determined by the distance from O of configuration space points that have all particles jammed tightly together somewhere in Ω) for large N is

$$r_{\text{circ}} \sim \Delta_\nu N^{(\nu+2)/\nu} \tag{25}$$

where constant $\Delta_\nu > 0$ is N-independent. Thus

$$r_{\text{circ}}/r_{\text{in}} \sim 2^{1/2}\,\Delta_\nu N^{(\nu+2)/\nu} \tag{26}$$

so the polytope develops more and more protuberance as N increases.

2.4. Bounds on Polytope Content

The behavior of the high-compression Helmholtz free energy per particle as $N \to \infty$ (the so-called "thermodynamic limit") can be inferred from Eq. (14):

$$\beta F_N/N \sim \nu \ln(\lambda/a) - \nu \ln[(\Omega/\Omega_0) - 1] + C_\nu \tag{27}$$

where

$$C_\nu = \nu \ln \nu - \lim_{N\to\infty} [\ln P_N^{(\nu)}/N] \tag{28}$$

Equation (27) represents the beginning of an asymptotic development appropriate at high compression,[10–12] with succeeding terms proportional to positive integral powers of $[(\Omega/\Omega_0) - 1]$.

The additive free-energy constant C_1 for rigid rods can easily be determined by integrating the exact Tonks equation of state[13, 14] with respect to density. One obtains

$$C_1 = -1 \tag{29}$$

Similar exact results are not known at present for $\nu > 1$. However, reasonably good estimates for C_2 are available both from molecular dynamics machine computations of the rigid disk equation of state,[3,15] as well as the purely theoretical cell-cluster technique,[11] so we may tentatively conclude

$$C_2 = 0.10 \pm 0.02 \tag{30}$$

For rigid spheres C_3 should in principle depend on the type of packing (f.c.c., h.c.p., or hybrid), but both the molecular dynamics and cell-cluster methods agree that the difference is very small. Thus for any sphere close packing, References 11, 14, and 15 imply

$$C_3 = 1.78 \pm 0.02 \tag{31}$$

There is some evidence[8,12] that

$$C_3(\text{h.c.p.}) < C_3(\text{f.c.c.}) \tag{32}$$

with the difference between them of the order of 10^{-3}.

The uncertainties about magnitudes of C_2 and the C_3's make it desirable to find upper and lower bounds on these quantities. This can be done by computing the contents of suitable inscribed and circumscribed bodies for $P_N^{(\nu)}$, respectively. The obvious first choices are the inscribed and circumscribed hyperspheres discussed in Section 2.3. From the general formula for the content V_n of an n-dimensional hypersphere with radius r,[16]

$$V_n(r) = \frac{2\pi^{n/2} r^n}{n\Gamma(n/2)} \tag{33}$$

the inscribed and circumscribed bounds

$$V_{\nu(N-1)}(r_{\text{in}}) < P_N^{(\nu)} < V_{\nu(N-1)}(r_{\text{circ}}) \tag{34}$$

lead, with use of Stirling's asymptote to the gamma function for large N, to the bounds

$$\frac{\nu}{2} \ln\left[\frac{\pi e}{\nu N}\right] \lesssim \frac{\ln P_N^{(\nu)}}{N} \lesssim \frac{\nu}{2} \ln\left[\frac{\pi e\, \Delta_\nu N^{2/\nu}}{\nu}\right] \tag{35}$$

As $N \to \infty$, we see by comparing (28) with (35) that the use of inscribed and circumscribed hyperspheres succeeds only in bounding the C_ν by plus and minus infinity. This failure to produce useful bounds is a further reflection of the extreme protuber-

ance of the large-N polytopes, and it suggests that similarly protuberant bodies must be used to construct sensible bounds.

Fortunately such protuberant bodies can be found. Indeed, Salsburg[17] has previously shown that removal of certain faces from $P_N^{(\nu)}$ for rigid disks and spheres in f.c.c. packing followed by extension of the remaining faces till they meet results in a larger polytope whose content may be found exactly by elementary means. The trick is to retain only those interactions for neighbors which are aligned parallel to two fundamental crystal directions for $\nu = 2$, or three for $\nu = 3$. The situation is illustrated in Fig. 4. After transformation to the type of oblique coordinates shown in that figure for each particle, the entire configuration integral factors into those for sets of one-dimensional rigid rods. [The fixed center-of-mass constraint may readily be taken into account, but has no effect as $N \to \infty$.] We refer the reader to Reference 17 for details, and merely quote the results:

$$C_2 \geqslant \ln\left(\frac{2\sqrt{3}}{e^2}\right) = -0.7575... \tag{36}$$

$$C_3(\text{f.c.c.}) \geqslant \ln\left(\frac{27}{\sqrt{2}\, e^3}\right) = -0.05074... \tag{37}$$

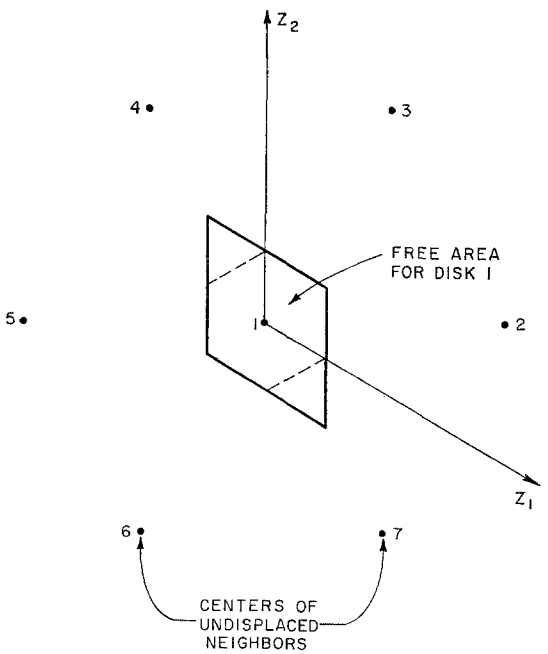

Fig. 4. Neglected rigid disk interactions for lower bound [Eq. (36)] to C_2. The rhombus shown is the free area available to central particle 1 when repulsions due to 4 and 7 are disregarded. When all interactions for pairs oriented parallel to (1,4) and (1,7) are dropped, the configuration integral in the oblique coordinate system z_1, z_2 factors into rigid-rod-type configuration integrals. In the f.c.c. sphere crystal, only pair interactions along three of the six possible directions are retained.

Unfortunately no way is known to systematically improve these lower bounds. Also, the method totally fails for the h.c.p. sphere crystal because that system does not have three noncoplanar lines of nearest-neighbor particles passing through every sphere position, as the f.c.c. lattice does.

The situation is somewhat brighter so far as upper bounds are concerned. The most obvious possibility arises by confining the particles to the so-called "Kirkwood" free areas (for $\nu = 2$) or free volumes (for any $\nu = 3$ crystal). These regions are the largest identical convex regions over which the particles may wander from their regular lattice sites without particle collisions occurring. They are generated by replacing each condition (11) by the more stringent *pair* of conditions

$$\begin{aligned} \tfrac{1}{2} + \mathbf{w}_{ij} \cdot \mathbf{t}_j &\geqslant 0 \\ \tfrac{1}{2} - \mathbf{w}_{ij} \cdot \mathbf{t}_i &\geqslant 0 \end{aligned} \tag{38}$$

These new restraints force rigid disks to stay within small regular hexagons, all of equal size; in the $\nu = 3$ cases the analogous Kirkwood free volumes are dodecahedra. Reference 17 again outlines the detailed calculation. The results are

$$C_2 \leqslant \ln(8/\sqrt{3}) = 1.5301... \tag{39}$$

$$C_3(\text{f.c.c.}),\ C_3(\text{h.c.p.}) \leqslant \ln(27\sqrt{2}) = 3.6424... \tag{40}$$

The equality of the estimates for the f.c.c. and h.c.p. crystals is due to the fact that the Kirkwood regions have identical volumes, as a very simple argument demonstrates.[10]

A slight improvement upon these simple upper bounds is possible by using Barker's tunnel model idea.[18] Thus, collision conditions (11) are all replaced by pairs of conditions (38) *except* for all pairs parallel to a fundamental crystal direction characterized by lines of neighboring particles. [Since only one such line direction is required, the h.c.p. sphere crystal can be included; such lines of particles occur in the basal plane.] The lines of particles along which the true pair collisions are permitted to occur constitute essentially a one-dimensional system of particles "in a tunnel." Calculation of the relevant "tunnel" partition function requires finding the largest eigenvalue of a degenerate integral operator. For rigid disks one ultimately obtains[17]

$$C_2 \leqslant \ln[12(\sqrt{12} - \sqrt{10})] = 1.2869... \tag{41}$$

Rudd[19] has carried out the analogous calculation for the three-dimensional crystals, with a common result for f.c.c. and h.c.p. cases:

$$C_3(\text{f.c.c.}),\ C_3(\text{h.c.p.}) \leqslant 3.5044... \tag{42}$$

The tunnel partitioning of the crystal particles apparently does not grant them very much more freedom of motion than do the Kirkwood free volumes, especially in three dimensions. A better procedure is to partition the particles into compact finite groups, retaining conditions (11) for interactions within each group, but making the replacement (38) for interactions between particles in different groups. This has the

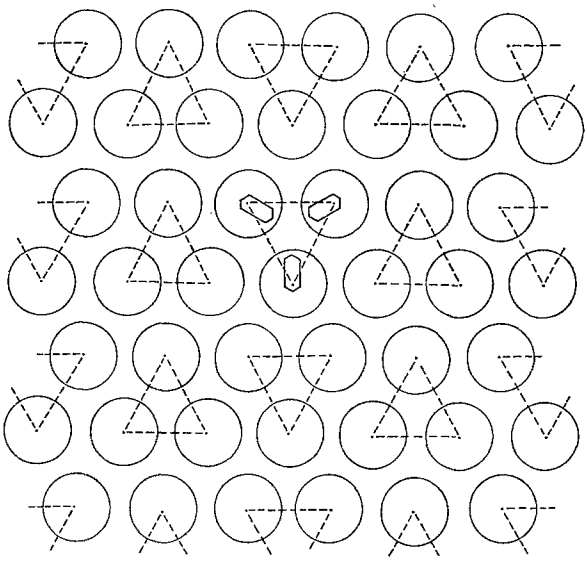

Fig. 5. Triangular partitioning of the rigid disk crystal for establishing upper bound (43) on C_2. The elongated hexagons represent the limits of movement for particles in one of the compact groupings.

effect of decoupling the groups from one another, allowing upper estimates to the free energy in terms of configurational integrals just for the small compact groups.

Figure 5 shows the simplest rigid disk partitioning, triangular groups of three particles. The related configurational integral can be evaluated exactly by techniques devised for the cell-cluster theory,[10] and it leads to the following improved bound:

$$C_2 \leqslant 1.1678 \tag{43}$$

The rhombic grouping of four disks does even better:

$$C_2 \leqslant 1.0623 \tag{44}$$

and systematic continuation of this procedure with larger and larger compact groups would eventually converge onto the exact C_2.

In order to achieve results in three dimensions comparable to (43) in tightness as a bound, we anticipate that tetrahedral clusters of four spheres would be required. Interestingly, the results should differ for f.c.c. and h.c.p. crystals.

3. GEOMETRIC INTERPRETATION OF PAIR CORRELATION FUNCTIONS

3.1. Polytope Sections

Unlike the situation for systems bounded by impenetrable walls, our crystals subject to periodic boundary conditions have spatially constant singlet distribution

functions equal to the overall density N/Ω. The crystalline order manifests itself only in the higher-order distribution functions. The important pair distribution function $\rho^{(2)}(\mathbf{r})$, for example, will depend upon the direction of $\mathbf{r}$ in a manner consistent with the basic symmetry of the crystal involved.

For certain purposes it is unnecessary to consider the complete function $\rho^{(2)}(\mathbf{r})$. Instead, it is convenient and sufficient to examine the orientational average of $\rho^{(2)}(\mathbf{r})$, which introduces the radial pair correlation function $g^{(2)}(r)$:

$$\langle \rho^{(2)}(\mathbf{r}) \rangle_{\text{orientations}} = [N(N-1)/\Omega^2]\, g^{(2)}(r) \tag{45}$$

This latter function may easily be expressed as a configuration-space average (for $r > 0$):

$$\begin{aligned} A_\nu(r)\, g^{(2)}(r) &= \frac{\Omega \int_\Omega d\mathbf{r}_1 \cdots \int_\Omega d\mathbf{r}_N \left[\sum_{i,j=1}^N \delta(r - r_{ij})\right] \prod_{k<l=1}^N U(r_{kl} - a)}{N(N-1) \int_\Omega d\mathbf{r}_1 \cdots \int_\Omega d\mathbf{r}_N \prod_{k<l=1}^N U(r_{kl} - a)} \\ A_\nu(r) &= \frac{dV_\nu(r)}{dr} = \frac{2\pi^{\nu/2} r^{\nu-1}}{\Gamma(\nu/2)} \end{aligned} \tag{46}$$

where we have used notation analogous to that for partition function (2).

In the high-compression regime, as previously remarked, the available configuration space separates into $(N-1)!$ hyperprisms, differing only by particle permutations. Since the separate hyperprisms give identical contributions to the numerator integral in (46), with a similar circumstance for the denominator integral, we may restrict both integrals to one hyperprism $H_N^{(\nu)}$ alone:

$$A_\nu(r)\, g^{(2)}(r) = \frac{\Omega \int_{H_N^{(\nu)}} d\mathbf{r}_1 \cdots d\mathbf{r}_N \left[\sum_{i,j=1}^N \delta(r - r_{ij})\right]}{N(N-1) \int_{H_N^{(\nu)}} d\mathbf{r}_1 \cdots d\mathbf{r}_N} \tag{47}$$

Furthermore, the fact that each delta function depends only on the relative distance between particles means that the system center of mass may be held fixed in both numerator and denominator of (47); the integrals then will span only the $[\nu(N-1)]$-dimensional cross section $S_N^{(\nu)}$ of the hyperprism:

$$A_\nu(r)\, g^{(2)}(r) = \frac{\Omega}{N(N-1)\, S_N^{(\nu)}} \int_{S_N^{(\nu)}} d^{\nu(N-1)}\mathbf{r} \left[\sum_{i,j=1}^N \delta(r - r_{ij})\right] \tag{48}$$

Under high compression the variable transformation (12) from $\mathbf{r}_1, \ldots, \mathbf{r}_N$ to $\mathbf{t}_1, \ldots, \mathbf{t}_N$ becomes appropriate, and in the new basis, polytope $P_N^{(\nu)}$ is asymptotically the correct integration region. In addition we have

$$\begin{aligned} r_{ij} &\sim \mathbf{w}_{ij} \cdot (\mathbf{r}_{ij}^{(0)} + \delta\mathbf{r}_j - \delta\mathbf{r}_i) \\ &= \mathbf{w}_{ij} \cdot \mathbf{r}_{ij}^{(0)} + \frac{a}{\nu}\left(\frac{\Omega}{\Omega_0} - 1\right) \mathbf{w}_{ij} \cdot (\mathbf{t}_j - \mathbf{t}_i) \end{aligned} \tag{49}$$

Consequently the radial pair correlation function may be expressed thus:

$$A_\nu(r)\, g^{(2)}(r) = \frac{\Omega}{N(N-1)\, P_N^{(\nu)}} \int_{P_N^{(\nu)}} d^{\nu(N-1)}\mathbf{t} \left\{ \sum_{i,j=1}^{N} \delta \left[r - \mathbf{w}_{ij} \cdot \mathbf{r}_{ij}^{(0)} - \frac{a}{\nu}\left(\frac{\Omega}{\Omega_0} - 1\right) \mathbf{w}_{ij} \cdot (\mathbf{t}_j - \mathbf{t}_i) \right] \right\} \tag{50}$$

Because the particles on the average deviate so little from their nominal lattice sites $\mathbf{r}_i^{(0)}$, when the system is nearly close-packed, $g^{(2)}(r)$ will be different from zero substantially only when r is in the immediate vicinity of one of the lattice distances $|\, \mathbf{r}_{ij}^{(0)}\, |$. In other words, it will strongly exhibit the existence of discrete shells of neighbors. For this reason we may let $z_{\nu n}$ stand for the number of nth nearest neighbors ($z_{\nu 1} = z_\nu$), and then rewrite Eq. (50) in a form which explicitly indicates the coordination shells:

$$A_\nu(r)\, g^{(2)}(r) = \frac{\Omega\nu}{(N-1)\, a[(\Omega/\Omega_0) - 1]} \sum_{n=1}^{\infty} z_{\nu n} g_{\nu n} \left[\frac{\nu}{a}\left(\frac{\Omega}{\Omega_0} - 1\right)^{-1} (r - r_{1,n+1}^{(0)}) \right] \tag{51}$$

Here, the nth coordination shell peak function $g_{\nu n}$ is defined to be

$$g_{\nu n}(x) = \frac{1}{P_N^{(\nu)}} \int_{P_N^{(\nu)}} d^{\nu(N-1)}\mathbf{t}\, \delta[x - \mathbf{w}_{1,n+1} \cdot (\mathbf{t}_{n+1} - \mathbf{t}_1)] \tag{52}$$

and we have presumed that particle $n + 1$ is an nth shell neighbor to particle 1.

The nearest-neighbor shell peak function $g_{\nu 1}(x)$ has a special prominence by virtue of the virial equation of state for ν-dimensional rigid spheres:[1]

$$\frac{\beta p \Omega}{N} = 1 + \frac{(N-1)a}{2\Omega\nu} A_\nu(a)\, g^{(2)}(a + 0) \tag{53}$$

where the pressure is

$$p = -\left(\frac{\partial F_N}{\partial \Omega}\right)_{N,\beta} \tag{54}$$

The substitution of (51) into (53) yields

$$\frac{\beta p \Omega}{N} \sim 1 + \tfrac{1}{2} z_{\nu 1} g_{\nu 1}(-1 + 0)[(\Omega/\Omega_0) - 1]^{-1} \tag{55}$$

where we have used the high-compression identity

$$(a/\nu)[(\Omega/\Omega_0) - 1] = r_{12}^{(0)} - a \tag{56}$$

The pressure may also be calculated from the free-energy expression (14) with the result

$$\beta p \sim \frac{\nu(N-1)}{\Omega_0}\left(\frac{\Omega}{\Omega_0} - 1\right)^{-1} \tag{57}$$

which is the ν-dimensional form of the free-volume equation of state.[5] Comparison of Eqs. (53) and (57) gives

$$g_{\nu 1}(-1+0) = \frac{2\nu(N-1)}{z_{\nu 1}N} \tag{58}$$

Since the argument of $\delta[\cdots]$ in definition (52) of $g_{\nu n}(x)$ is linear in the t's, this delta function will be nonvanishing only on a $[\nu(N-1)-1]$-dimensional hyperplane intersecting polytope $P_N^{(\nu)}$. The integral then gives $K_{\nu n}C_{\nu n}(x)$, where $K_{\nu n}$ is a positive constant and $C_{\nu n}(x)$ is the cross-sectional "area" of $P_N^{(\nu)}$ in that hyperplane. [One can readily show that all $K_{\nu n}$ equal $2^{-1/2}$.] Equation (51) therefore shows us that the high-compression radial pair correlation function is synthesized from a set of cross sections through the polytope, taken in different directions for the separate shells of neighbors. Since

$$P_N^{(\nu)} = \int_{-\infty}^{+\infty} C_{\nu n}(x)\, d(K_n x) \tag{59}$$

we have the obvious peak function normalization conditions

$$1 = \int_{-\infty}^{+\infty} g_{\nu n}(x)\, dx \tag{60}$$

Inequality (11) shows that the nearest-neighbor function $g_{\nu 1}(x)$ vanishes identically for $x < -1$. For these values of x, the hyperplane fails to intersect the polytope. When $x = -1$, the sectioning hyperplane is exactly coincident with the (1, 2) polytope face, so that at this point $C_{\nu 1}(x)$ discontinuously jumps from zero to a positive value equal to the face content. As x increases above -1, the hyperplane moves across the polytope, always remaining parallel to the (1, 2) face, and $C_{\nu 1}(x)$ varies accordingly. Eventually x will become so large that the hyperplane moves completely across $P_N^{(\nu)}$ and out the other side, at which point, $x_{\max}$, $C_{\nu 1}(x)$ has declined to zero and remains zero thereafter. Figure 6 offers a schematic diagram of this sectioning process for the nearest-neighbor peak.

The analytic character of $g_{\nu 1}(x)$ for $\nu = 1$ (rigid rods on a line) may now be derived by extremely simple geometric means. In this case $P_N^{(1)}$ is a simplex, as has already been pointed out, and the entire family of nonvanishing cross sections $C_{1,1}(x)$ for all $-1 \leqslant x < x_{\max}$ have the same shape as the (1, 2) face, $C_{1,1}(-1)$. Therefore

$$C_{1,1}(x) = K[1 - (x/x_{\max})]^{N-2} \tag{61}$$

where K is a suitable positive constant. It is easy to establish that

$$x_{\max} = N - 1 \tag{62}$$

Therefore when the number N of particles is very large,

$$\begin{aligned} C_{1,1}(x) &= K\left(1 - \frac{x}{N-1}\right)^{N-2} \\ &\sim K\exp(-x) \end{aligned} \tag{63}$$

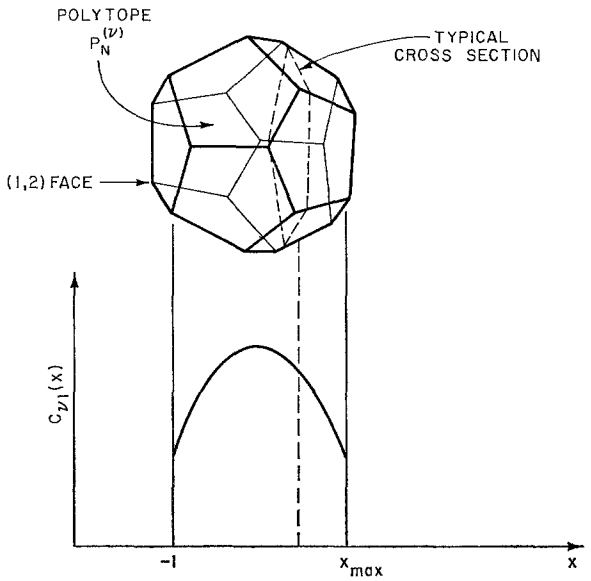

Fig. 6. Family of cross sections $C_{\nu 1}(x)$ for the nearest-neighbor peak of $g^{(2)}(r)$. The multidimensional polytope has schematically been represented as a dodecahedron, and the sectioning hyperplane is a conventional plane parallel to the (1,2) face ($x = -1$).

by employing the well-known product representation of the exponential function. K may be evaluated by comparison with Eq. (58), and so we conclude that as $N \to \infty$,

$$\begin{aligned} g_{1,1}(x) &= \exp(1 - x), \qquad x \geqslant -1 \\ &= 0 \qquad\qquad\quad x < -1 \end{aligned} \tag{64}$$

In conjunction with Eq. (51) for $g^{(2)}(r)$, we see that the known exponential character of the rigid rod nearest-neighbor distribution function[20] has a straightforward geometric interpretation.

Unfortunately, when $\nu > 1$ we cannot deduce geometrically (or any other way) the exact $N \to \infty$ analytic form of $g_{\nu 1}(x)$. Nevertheless, we know that this quantity always suffers a discontinuity at $x = -1$ as the sectioning hyperplane enters $P_N^{(\nu)}$. In addition, some further qualitative features will be established in Sections 4 and 5.

Consider an uninterrupted row of m particles in a crystal (ν arbitrary), which we will suppose are serially numbered 1 to m, with the end particles being nth nearest-neighbors ($m = n + 1$ only when $\nu = 1$). The unit vectors connecting adjacent particles in this sequence are equal:

$$\mathbf{w}_{12} = \mathbf{w}_{23} = \cdots = \mathbf{w}_{m-1,m} \tag{65}$$

Equation (52) shows that the hyperplane forming the related nth neighbor cross sections $C_{\nu n}(x)$ for this row is determined by

$$\begin{aligned} 0 &= x - \mathbf{w}_{12} \cdot (\mathbf{t}_m - \mathbf{t}_1) \\ &= x - \mathbf{w}_{12} \cdot [(\mathbf{t}_m - \mathbf{t}_{m-1}) + (\mathbf{t}_{m-1} - \mathbf{t}_{m-2}) + \cdots + (\mathbf{t}_2 - \mathbf{t}_1)] \end{aligned} \tag{66}$$

The configuration-space vector

$$\mathbf{T}^* = \mathbf{t}_{12}^* + \mathbf{t}_{23}^* + \cdots + \mathbf{t}_{m-1,m}^* \tag{67}$$

formed from the face normals defined by Eqs. (19) and (20) is normal to the cross sections $C_{\nu n}(x)$. The symmetrical form shown for $\mathbf{T}^*$ indicates that this vector is inclined at the same angle to each of $\mathbf{t}_{12}^*$, $\mathbf{t}_{23}^*$,..., $\mathbf{t}_{m-1,m}^*$. Consequently, when the hyperplane enters $P_N^{(\nu)}$ with increasing x, it does so at the confluence of these $m - 1$ faces, which is actually a $[\nu(N-1) - (m-1)]$-dimensional polytope.

By using the same schematic pictorialization for $P_N^{(\nu)}$ as a dodecahedron that appears in Fig. 6, we have exhibited in Fig. 7 the way in which the sectioning hyperplane enters $P_N^{(\nu)}$ for $m = 2, 3$, and 4. When $m = 2$, we have the previous case of nearest neighbors for which the hyperplane enters suddenly through an entire face. With $m = 3$, the hyperplane is symmetrically disposed with respect to two faces, and entrance occurs through an edge. For $m = 4$, involving three mutually intersecting faces, the hyperplane enters through a vertex. The significant point is that the initial rise from zero of the cross section increases by one algebraic degree for each extra face involved; for $m = 2$ there is a jump discontinuity (degree 0), for $m = 3$ there is a linear increase initially (degree 1), and for $m = 4$ the initial behavior is quadratic (degree 2).

Our diagrams in Fig. 7 fail to permit representation of the situation for rows of more than four particles. Nevertheless, it is clear that the general-m case produces in the actual polytope $P_N^{(\nu)}$ a cross section whose magnitude initially rises as an $(m-2)$-degree curve. Not only is this in accord with the known behavior of the rigid-rod

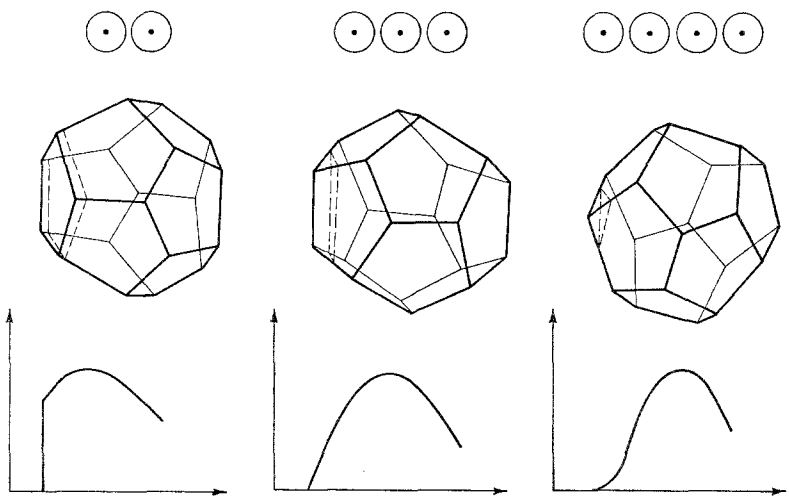

Fig. 7. Initial rise of radial pair correlation peaks for successively longer rows of particles. As outlined by dashed boundaries, the sectioning "hyperplane" enters the "polytope" at regions of decreasing dimensionality as the row length increases from $m = 2$. The behavior of the cross section magnitudes is indicated by the graphs at the bottom, with a jump discontinuity for $m = 2$, linearity for $m = 3$, and quadratic behavior for $m = 4$.

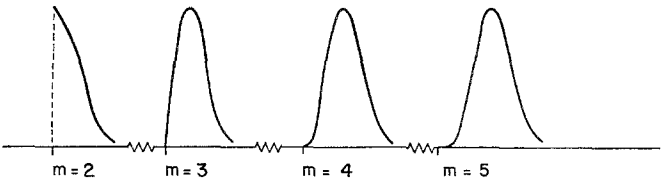

Fig. 8. Wood's results for rigid-disk pair correlation along a row of particles. The successive peaks are normalized to have the same maximum for convenience. The system consisted of $N = 192$ rigid disks (12×16 rectangular periodicity cell) at $p\Omega_0/Nk_BT = 40$, $(\Omega/\Omega_0) - 1 = 0.05$.

system,[20] but it can be observed as well in electronic-computer simulations of rigid-particle many-body systems. Figure 8, for instance, shows some high-pressure rigid-disk calculations kindly furnished us by Dr. William W. Wood that were obtained by the Monte Carlo method applied to 192 particles. The peak functions for rows of $m = 2$, 3, 4, and 5 disks are shown, and the increasing algebraic degree of the initial rises is very obvious. The importance of our geometric point of view is that it can easily identify the reason for this phenomenon without the necessity of finding an exact solution to the many-body problem involved. In retrospect it verifies the intuitive suspicion that a row of particles for $\nu > 1$ should behave in a rigid-rod-like fashion.

3.2. Geometric Meaning of the Born–Green–Yvon Equation

Now that we have an interpretation of the radial pair correlation function in terms of polytope sections, we may proceed with a geometric analysis of the rate of change of the sections as they move across the polytope. This will help us to uncover the geometrical content of the Born–Green–Yvon integrodifferential equation.[21] For the sake of concreteness, attention will initially be confined to the behavior of the nearest-neighbor peak; the generalization, however, will be very clear and straightforward after this one special case is worked out.

We have just established that the sectioning hyperplane enters $P_N^{(\nu)}$ through a face for the nearest-neighbor peak. Furthermore we recall that for large N the overwhelming majority of other polytope faces will be perpendicular to this one entrance face, say, the (1, 2) face. If it were true that *all* other faces were perpendicular to the (1, 2) face, then the magnitude of the cross section would not change (nor would its shape) as the sectioning hyperplane moved inward through $P_N^{(\nu)}$. After its initial discontinuity at $x = -1$, the peak function $g_{\nu 1}(x)$ accordingly would be a positive constant. This hypothetical situation is illustrated in three-dimensional analogy in Fig. 9.

The fact that $g_{\nu 1}(x)$ is not independent of x for $x > -1$ [as Eq. (64) demonstrates in the $\nu = 1$ case], therefore is attributable to contributions of the few faces not perpendicular to the (1, 2) face. The precise angle between the pairs of faces is decisive; if the angle between the outward normals is less than $\frac{1}{2}\pi$, the face contributes to a rise in $g_{\nu 1}(x)$ as x increases, and if the angle between the outward normals is more than $\frac{1}{2}\pi$, the contribution is toward a decrease in $g_{\nu 1}(x)$ with x.

Figure 10 should aid in formulating a precise statement of these facts. For a small increment Δx in variable x above the face-entering value $x = -1$, the cross section

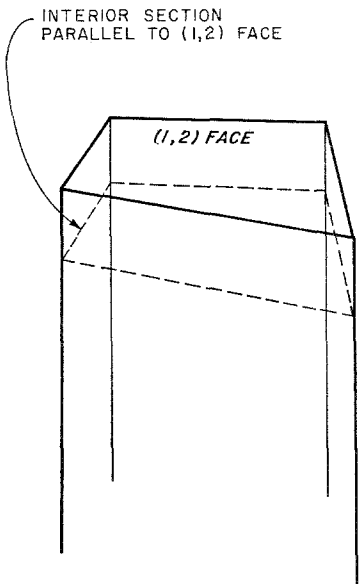

Fig. 9. Hypothetical $P_N^{(\nu)}$ geometry, with all other faces perpendicular to the (1,2) face. Interior sections in a hyperplane parallel to the (1,2) face all have exactly the same size and shape as that face.

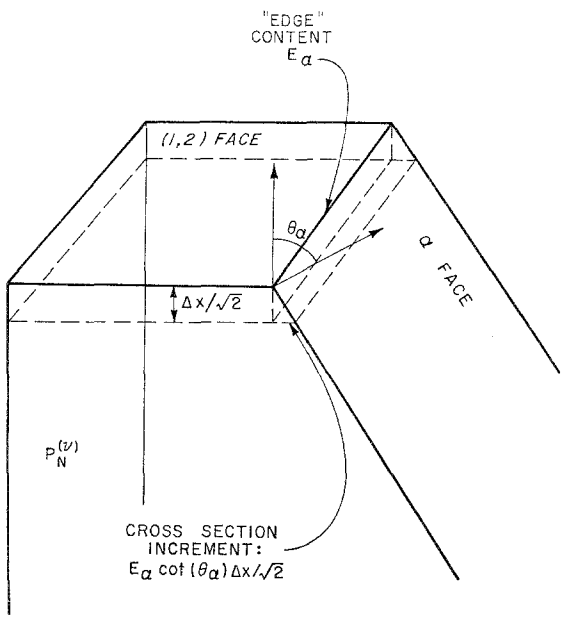

Fig. 10. Contribution of a nonperpendicular face [the (α) face] to cross section rate of change. For the case shown, $\theta_\alpha < \frac{1}{2}\pi$, the cross section increases as the hyperplane moves deeper into the polytope.

will have moved a distance $2^{-1/2}\,\Delta x$ into the polytope. [Recall that the face itself, $x = -1$, is only a distance $2^{-1/2}$ from the polytope center (at $x = 0$).] The change in cross section $C_{\nu 1}$ for sufficiently small Δx will consist of additive contributions from the "edges" E_α of face (1, 2) formed by intersection with the other faces. Specifically,

$$C_{\nu 1}(-1 + \Delta x) = C_{\nu 1}(-1) + 2^{-1/2}\,\Delta x \sum_\alpha E_\alpha \cot\theta_\alpha + O[(\Delta x)^2] \tag{68}$$

where θ_α is the angle between the outward normals to the (1, 2) face and the (α) face. This linear estimate merely adds up the content of the small hyperrectangles that are created ($\theta_\alpha < \frac{1}{2}\pi$) or destroyed ($\theta_\alpha > \frac{1}{2}\pi$) at the edges of $C_{\nu 1}(x)$ as it moves inward from $x = -1$; Fig. 10 shows in three-dimensional version one such thin "hyperrectangle." Note that since $\cot\frac{1}{2}\pi = 0$, the faces perpendicular to the (1, 2) face automatically give no contribution to (68) in the linear order shown.

Next we require a physical interpretation of the $[\nu(N-1)-2]$-dimensional "edges" E_α of the (1, 2) face. More generally, we shall identify $E_\alpha(\Delta x, \Delta x_\alpha)$, the "edge length" along which two hyperplane cross sections that are respectively parallel to the (1, 2) face and a distance $2^{-1/2}\,\Delta x$ beneath it, and parallel to the (α) face and a distance $2^{-1/2}\,\Delta x_\alpha$ beneath this other face, intersect. When the system configuration point lies on this more general edge, it is clear that the (1, 2) and the (α) pairs have been constrained to the pair separations indicated, and so $E_\alpha(\Delta x, \Delta x_\alpha)$ must be proportional to the related triplet distance probability.

If the (α) face were perpendicular to the (1, 2) face, then $2^{-1/2}\,\Delta x$ and $2^{-1/2}\,\Delta x_\alpha$ would be orthogonal coordinates, and the total polytope content would be obtained merely as a double integral of E_α:

$$P_N^{(\nu)} = \int_0^\infty d(2^{-1/2}\,\Delta x) \int_0^\infty d(2^{-1/2}\,\Delta x_\alpha)\, E_\alpha(\Delta x, \Delta x_\alpha) \tag{69}$$

However, greater interest attaches to the case of nonperpendicularity. In terms of the previously defined angle θ_α between face normals, Eq. (69) can be generalized by inclusion of transformation Jacobian $\csc\theta_\alpha$ for the now-oblique coordinates:

$$P_N^{(\nu)} = \int_0^\infty d(2^{-1/2}\,\Delta x) \int_0^\infty d(2^{-1/2}\,\Delta x_\alpha)\, \csc\theta_\alpha E_\alpha(\Delta x, \Delta x_\alpha) \tag{70}$$

Formula (69) is just a special case of this last expression. But now it becomes clear that

$$p_\alpha^{(3)}(\Delta x, \Delta x_\alpha) = \frac{E_\alpha(\Delta x, \Delta x_\alpha)}{2\sin\theta_\alpha P_N^{(\nu)}}\,. \tag{71}$$

is precisely the probability density for simultaneous pair separations Δx and Δx_α, for

$$1 = \int_0^\infty d(\Delta x) \int_0^\infty d(\Delta x_\alpha)\, p^{(3)}(\Delta x, \Delta x_\alpha) \tag{72}$$

We have included the superscript (3) since for the cases of importance in Eq. (68), the pairs (1, 2) and (α) will share a particle, and will hence include only three particles altogether.

Now substitute from Eq. (71) into the linear estimate (68):

$$C_{\nu 1}(-1+\Delta x) \cong C_{\nu 1}(-1) + 2^{1/2}\Delta x P_N^{(\nu)} \sum_\alpha \cos\theta_\alpha p_\alpha^{(3)}(\Delta x = 0, \Delta x_\alpha = 0) \quad (73)$$

Since the nearest-neighbor peak function is

$$g_{\nu 1}(x) = \frac{C_{\nu 1}(x)}{2^{1/2} P_N^{(\nu)}} \quad (74)$$

we have

$$\frac{g_{\nu 1}(-1+\Delta x) - g_{\nu 1}(-1)}{\Delta x} = \sum_\alpha \cos\theta_\alpha p_\alpha^{(3)}(0,0) \quad (75)$$

In the small-Δx limit, the left-hand member of this last relation passes over to an x derivative. If we furthermore use Eq. (23) to express $\cos\theta_\alpha$ in terms of the unit lattice vectors, Eq. (75) becomes

$$\frac{d\ln g_{\nu 1}(x)}{dx}\bigg|_{x=-1} = -\frac{1}{2}\sum_i{}' (\mathbf{w}_{i1}\cdot\mathbf{w}_{12})\frac{p_{i1}^{(3)}(0,0)}{g_{\nu 1}(-1)} - \frac{1}{2}\sum_j{}' (\mathbf{w}_{12}\cdot\mathbf{w}_{2j})\frac{p_{2j}^{(3)}(0,0)}{g_{\nu 1}(-1)} \quad (76)$$

The primes on the summations here indicate that particle i is a nearest neighbor of 1 (but $i \neq 2$), and that j is a nearest neighbor of 2 (but $j \neq 1$).

Equation (60) assures that $g_{\nu 1}(x)$ is a properly normalized distance distribution for the pair (1, 2) of nearest neighbors. The ratio $p_{i1}^{(3)}(0,0)/g_{\nu 1}(-1)$ therefore is the conditional probability that pair $(i, 1)$ be in contact, provided that (1, 2) is in contact, and an analogous statement applies to $p_{2j}^{(3)}(0,0)/g_{\nu 1}(-1)$. With these interpretations in mind, we can see that Eq. (76) is the high-density version of the Born–Green–Yvon integrodifferential equation,[21] for the left member is $(k_B T)^{-1}$ times the mean force acting between particles 1 and 2, and the right member specifies that this mean force is due to kinetic impulses provided by the set of neighbors of 1 and 2, with the scalar products of $\mathbf{w}$'s serving merely to project these collisional forces along the (1, 2) axis. [The conventional Born–Green–Yvon equation for hard spheres includes angular integrals over triplet conditional probabilities; since we only require distance-dependent $p^{(3)}$'s, these angles have been implicitly integrated out of Eq. (76). Furthermore the factors $\frac{1}{2}$ in (76) account for inclusion of all pair contacts with 1 and 2, rather than just one of them as is ordinarily the case for the Born–Green–Yvon equation.]

Equation (76) was derived for $x = -1$, when the relevant cross section $C_{\nu 1}$ just begins to enter $P_N^{(\nu)}$. The generalization to arbitrary x in $P_N^{(\nu)}$ is utterly straightforward. One uses the same type of linear estimate as (68) for the effect on $C_{\nu 1}(x)$ of a further small displacement $2^{-1/2}\Delta x$ into the polytope. One finds ($x > -1$):

$$\frac{d\ln g_{\nu 1}(x)}{dx} = -\frac{1}{2}\sum_i{}' (\mathbf{w}_{i1}\cdot\mathbf{w}_{12})\frac{p_{i1}^{(3)}(x+1,0)}{g_{\nu 1}(x)} - \frac{1}{2}\sum_j{}' (\mathbf{w}_{12}\cdot\mathbf{w}_{2j})\frac{p_{2j}^{(3)}(x+1,0)}{g_{\nu 1}(x)} \quad (77)$$

Now $p_{i1}^{(3)}(x+1,0)/g_{\nu 1}(x)$, for instance, is the conditional probability that $(i, 1)$ be in contact while the (1, 2) pair has reduced separation x. Of course the physical inter-

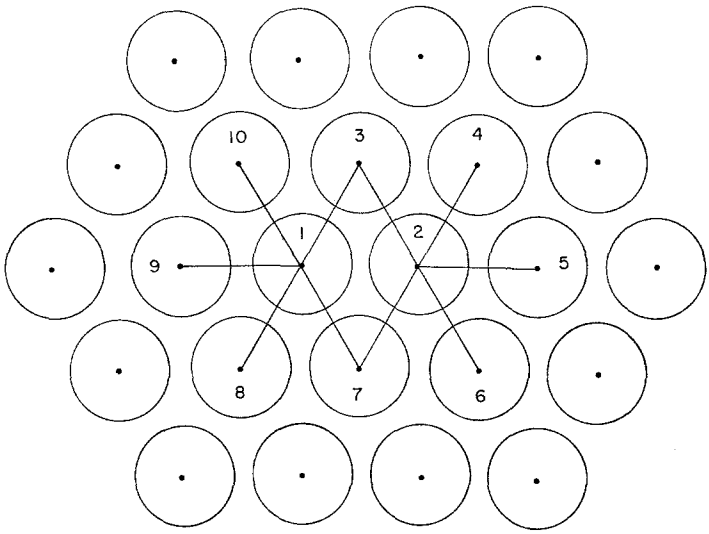

Fig. 11. Pair collisions that contribute to the distance distribution for a pair (1,2) of nearest-neighbor disks. Pairs (1,3), (1,7), (2,3), and (2,7) tend to drive particles 1 and 2 apart, while the others tend to drive them together.

pretation still persists that the mean force on pair (1, 2) is due to collisions with surrounding neighbors.

Figure 11 shows nearest-neighbor pair (1, 2) as rigid disks embedded in the surrounding crystal. One can see from the diagram that for $\nu > 1$ the right member of Eq. (77) contains both terms which tend to drive the (1, 2) pair together (positive scalar product of $\mathbf{w}$'s) and terms which tend to drive them apart (negative scalar product of $\mathbf{w}$'s).

If particles 1 and 2 had not initially been nearest neighbors, but were instead nth nearest neighbors ($n > 1$), we know that the relevant cross section $C_{\nu n}(x)$ would not enter the polytope across one of its faces, but along some other direction. It is straightforward to show that the only polytope faces not perpendicular to $C_{\nu n}$ are those corresponding as before to pairs (α) which include particle 1 or particle 2. In the same manner as before we may proceed to deduce the nth shell peak function Born–Green–Yvon equation:

$$\frac{d \ln g_{\nu n}(x)}{dx} = -\frac{1}{2}\sum_i{}' (\mathbf{w}_{i1} \cdot \mathbf{w}_{12}) \frac{p_{i1}^{(3)}(x+1, 0)}{g_{\nu n}(x)} - \frac{1}{2}\sum_j{}' (\mathbf{w}_{12} \cdot \mathbf{w}_{2j}) \frac{p_{2j}^{(3)}(x+1, 0)}{g_{\nu n}(x)} \tag{78}$$

The $p^{(3)}$'s now specify simultaneous occurrence of the non-nearest-neighbor (1, 2) distance, and a precise contact of a third particle with 1 or 2.

It may be mentioned in passing that analogous (but more elaborate) geometrical interpretations are also available for the orientationally unaveraged Born–Green–Yvon equation for the pair correlation function. Likewise this equation may also be similarly interpreted in the case of higher-order correlation functions.

4. EFFECT OF INCREASING DIMENSIONALITY

A few years ago Metropolis *et al.*[22] observed a fundamental structural difference between rigid-disk and rigid-sphere pair correlation functions under high compression. Their Monte Carlo calculations indicated that the nearest-neighbor peak function $g_{\nu,1}(x)$ has negative slope at $x = -1 + 0$ for $\nu = 2$ (disks), but positive slope at the same x for $\nu = 3$ (spheres). This means that two disks on contact experience a net average force due to their surroundings tending to hold them together, but in the case of spheres this mean force tends to pull them apart. The sphere function $g_{3,1}(x)$ thus passes through a maximum for $x > -1$, and reflects a greater tendency in three dimensions than in two for particles to be localized at regular crystal sites.

This structural difference has subsequently been confirmed by further Monte Carlo calculations by Rotenberg[23] and by Wood.[4] Also, Larsen and Salsburg[24,25] observed the same phenomenon in the cell-cluster theory for $g_{\nu,1}(x)$. Up to the present time, a statement in Reference 22 seemed an apt summation of the theoretical attitude toward the special crystal localization tendency exhibited by spheres: "Its occurrence in three dimensions is clearly a complex, many-body phenomenon, and we have not been able to fully explain it." The missing explanation can at least partially be revealed by our geometrical polytope theory.

The considerations of Section 3 show that the sign of the initial slope of $g_{\nu,1}(x)$ just beyond particle contact is generally established by competition between opposing contributions—some polytope faces are oriented so as to increase $g_{\nu,1}$ with increasing x, others to decrease it. Except for the rigid-rod case, for which only decreasing contributions occur, it is not at first obvious how the result of this competition goes as ν increases through 2, 3, 4,... . Nevertheless, the trend is determined by rather elementary considerations.

Certain general features of $g_{\nu 1}(x)$ are clear. Since $x < -1$ corresponds to overlap and thus vanishing of this function, the normalization condition (60) becomes

$$1 = \int_{-1}^{\infty} g_{\nu 1}(x)\, dx \tag{79}$$

Also, because $x = 0$ corresponds to the nominal lattice spacing in the crystal (i.e., all particles at the regular crystal sites), we expect $g_{\nu 1}(x)$ to go quickly to zero for x larger than 2 or 3. Thus the second moment or "width" of $g_{\nu 1}(x)$ should not increase beyond a number of order unity, even though $\nu \to \infty$. Finally, we shall establish in Section 5 that $g_{\nu 1}(x)$ passes through only a single maximum.

In the large-system limit, Eq. (58) gives

$$g_{\nu 1}(-1 + 0) = 2\nu/z_{\nu 1} \tag{80}$$

If $z_{\nu 1}$, the number of nearest neighbors, increases faster than ν, so that

$$\lim_{\nu \to \infty} 2\nu/z_{\nu 1} = 0 \tag{81}$$

then the contact value of $g_{\nu 1}(x)$ will decline to zero as $\nu \to \infty$. The only way this can happen while still maintaining normalization (79) and bounded width for a single-

maximum nonnegative function is for the initial slope $\partial g_{\nu 1}(-1+0)/\partial x$ to become positive. Loosely speaking, $g_{\nu 1}(x)$ would then be forced to increase from its very small value at contact.

We must thus inquire into the behavior of coordination number $z_{\nu 1}$ as ν increases. The structure of the densest packing of rigid n-dimensional spheres in Euclidean n-space is not generally known. In fact, it has been conjectured[26] that for sufficiently large n the densest packings are not even lattice packings (that is, not regular crystals, but amorphous structures). For present purposes it suffices to exhibit a hierarchy of lattice packings for which $z_{\nu 1}$ is easily determined; any denser packings presumably have higher numbers of nearest neighbors as x increases.

The relevant sequence of lattices is generated by a simple process that starts with rigid rods on a line. As shown in Fig. 12, the linear array of rods in contact may first be replaced by disks of equal diameter, then parallel translates of this line of touching disks may be generated so that as each new line of disks is created, it just fits on top of (or below) the previous line. The end result of the process is the close-packed hexagonal array of disks covering the plane.

Each disk in the new lattice thus formed touches two disks of the line just below

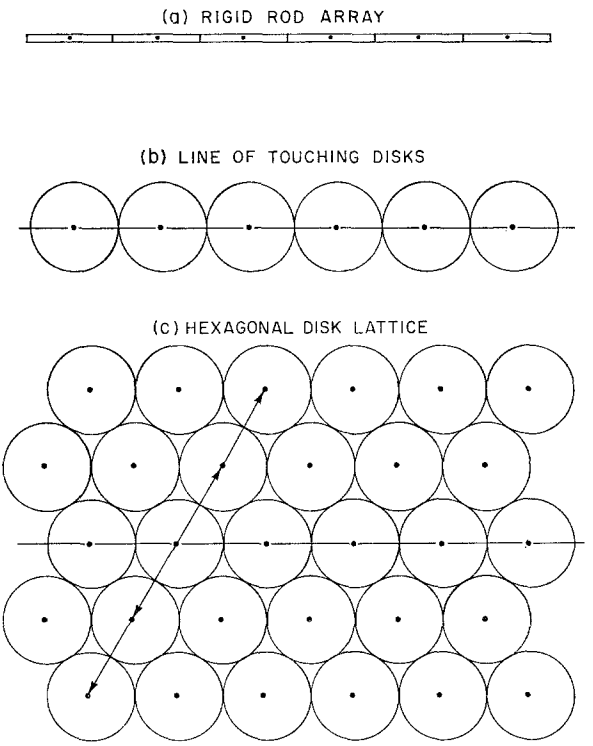

Fig. 12. Formation of the planar hexagonal disk packing from the linear array of rigid rods. First the rods are "expanded" into a linear sequence of touching disks. Then the line of disks is replicated by parallel displacements to form further lines of disks just fitting onto lines already placed. The arrows indicate the required oblique displacements.

it, and the three disk centers form a regular two-dimensional simplex, an equilateral triangle. The six nearest neighbors in the disk lattice consist of the two neighbors along the original line direction, plus two more each from the line above and the line below:

$$z_{2,1} = 2 + 2(2) \tag{82}$$

In order to create a lattice of spheres, an entirely analogous operation is carried out. First start with the planar disk lattice shown at the bottom of Fig. 12. Each disk is then expanded into a three-dimensional sphere with the same diameter. The resulting sphere layer is subsequently replicated by oblique displacements so that successive sphere layers are stacked one upon the other. If these oblique displacements are all integral multiples of a single displacement vector, the sphere packing has the face-centered cubic structure. Figure 13 indicates the formation of this packing, in which each sphere rests upon three others in the layer below to form a regular tetrahedron of centers.

In passing from rigid rods to rigid disks, the oblique displacements (see Fig. 12) are at such an angle (60°) to the original line that after every second replication or

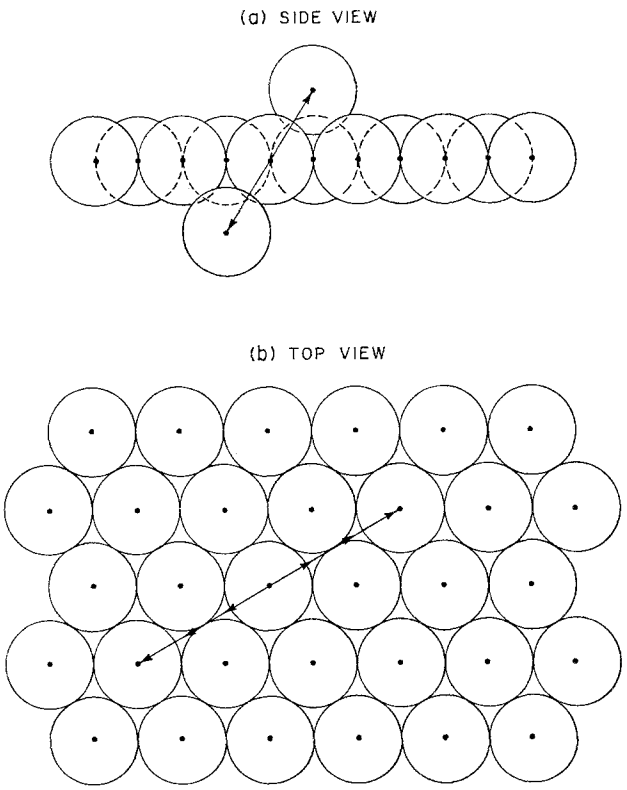

Fig. 13. Formation of the face-centered cubic lattice from the planar hexagonal disk packing. After the disks in the latter are expanded into spheres, the sphere layer is reproduced by oblique parallel translations (shown by the arrows).

displacement the disk centers lie directly above the original ones. The top view in Fig. 13 shows that in generation of the three-dimensional sphere lattice, *three* successive displacements are necessary before sphere centers lie directly above the starting set.

The twelve nearest neighbors in the face-centered cubic lattice may be divided up in a way analogous to (82):

$$z_{3,1} = z_{2,1} + 2(3) \tag{83}$$

First there are the $z_{2,1} = 6$ neighbors in the same layer. Then there are the three spheres above with which a given sphere forms the regular simplex (tetrahedron) and the three below.

Our procedure may be extended to form a lattice packing of hyperspheres in four dimensions. This is done by making each sphere in the face-centered cubic lattice into a hypersphere to form the initial "layer" of the four-dimensional packing. As before, this layer is subsequently replicated by oblique displacements to form further layers that fit on top of one another. Each hypersphere will fit upon four others in the layer below, and the five centers will form the vertices of a regular four-dimensional simplex. The number of nearest neighbors may be obtained from the analog of relation (83), namely:

$$\begin{aligned} z_{4,1} &= z_{3,1} + 2(4) \\ &= 12 + 8 = 20 \end{aligned} \tag{84}$$

By continuation of this process, we obtain a general difference relation satisfied by the coordination number $z_{\nu 1}$ in ν dimensions:

$$z_{\nu,1} = z_{\nu-1,1} + 2\nu \tag{85}$$

which represents the general term in sequence (82), (83), and (84). Using $z_{1,1} = 2$, we find the solution to this difference equation to be

$$z_{\nu,1} = \nu(\nu + 1) \tag{86}$$

This result verifies the zero limit postulated in Eq. (81), so that the initial slope of $g_{\nu 1}(x)$ must indeed become positive as ν increases from 1.

If one employs the known geometrical properties of hyperspheres and simplexes in spaces of arbitrary dimensionality, it is easy to show that the lattices generated by the above scheme have a packing fraction equal to

$$q(\nu) = \frac{\pi^{\nu/2}}{2^{\nu/2-1}\nu(\nu + 1)^{1/2}\Gamma(\nu/2)} \tag{87}$$

In other words, $q(\nu)$ is the fraction of ν-space interior to the hyperspheres. For $\nu > 3$, this last expression is actually smaller than the packing fractions listed by Rogers.[27] Presumably these more efficient packings have even larger coordinations than $z_{\nu,1}$ in Eq. (86), but that would only strengthen our argument about the initial slope.

The rapid increase of $z_{\nu,1}$ with ν very clearly *must* lead to increasing particle localization at nominal lattice sites. After all, it takes only $\nu + 1$ neighbors to trap a

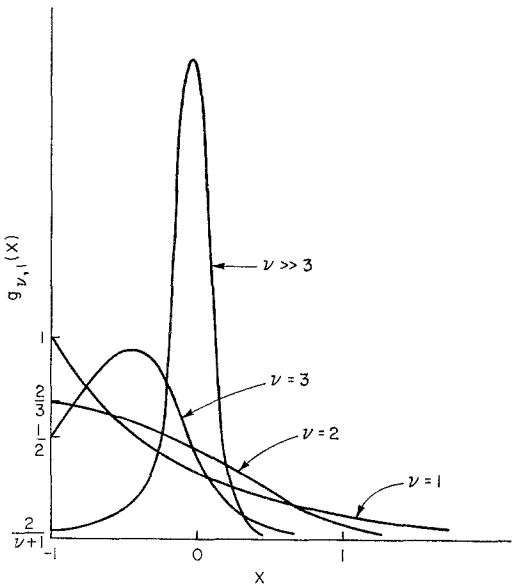

Fig. 14. Schematic trend of the first-neighbor peak function $g_{\nu,1}(x)$ as dimensionality increases. For rigid rods, $g_{1,1}(x)$ is a simple exponential, Eq. (64). As ν increases, the functions develop positive slope at $x = -1$, and tend to peak more and more sharply at $x = 0$ (the perfect crystal spacing).

central particle. As ν increases, this is a smaller and smaller fraction of the total number of neighbors, and the ones which will do the trapping are those which have wandered most closely toward the particle of interest. With a very large set of nearest neighbors, then, it becomes very probable that any one particle should be trapped close to its lattice site. As $\nu \to \infty$, we can therefore reasonably expect that $g_{\nu,1}(x)$ will become narrowly peaked about $x = 0$.[3] This trend is illustrated schematically in Fig. 14.

A similar peaking tendency for the other $g_{\nu,n}(x)$ should also obtain as $\nu + \infty$. In view of the polytope cross section interpretation of this set of functions, we see that for large ν the content of $P_N^{(\nu)}$ will be strongly concentrated around its centroid.

5. BRÜNN-MINKOWSKI INEQUALITY

Thus far, the convexity of limiting polytope $P_N^{(\nu)}$ has been employed only in the most superficial manner. The property of convexity nevertheless leads to a rather deep body of geometrical theory.[28] We shall now explore the implications of one particular aspect of that theory which has special relevance to the high-compression crystalline distribution functions.

A real-valued function $R(x)$ is said to be *concave* in the interval $[x_{\min}, x_{\max}]$ if for any x_1 and x_2 in this interval, the following inequality is valid:

$$R[(1 - \lambda)x_1 + \lambda x_2] \geqslant (1 - \lambda)\, R(x_1) + \lambda R(x_2) \tag{88}$$

[3] On the basis of a simple independent normal distribution of neighbor displacements, one estimates that the width of the $g_{\nu,1}(x)$ peak should be proportional to $(\ln \nu)^{-1/2}$ as $\nu \to \infty$, if Eq. (86) is correct.

for all $0 \leqslant \lambda \leqslant 1$. In graphical terms, this simply means that a straight line connecting two points of the R curve never lie above that curve. If R is concave it can therefore have no relative minima.

The central theorem to which we must appeal is the Brünn–Minkowski theorem.[29] It asserts the convexity of a certain hypervolume function in m-dimensional space that is formed by "addition" of two convex bodies $\mathbf{B}_1$ and $\mathbf{B}_2$ in that space. The body $\mathbf{B}$ in that space denoted by the "sum"

$$\mathbf{B}(\lambda) = (1 - \lambda)\mathbf{B}_1 + \lambda\mathbf{B}_2 \tag{89}$$

is the set of all points

$$\mathbf{r} = (1 - \lambda)\mathbf{r}_1 + \lambda\mathbf{r}_2 \tag{90}$$

where $\mathbf{r}_1$ is the position of a point in $\mathbf{B}_1$, and $\mathbf{r}_2$ is the position of a point in $\mathbf{B}_2$. $\mathbf{B}(\lambda)$ is known to be a convex body; its position and orientation perforce depend on those of $\mathbf{B}_1$ and $\mathbf{B}_2$, but not its size or shape.

Let $V_m[\mathbf{B}_\alpha]$ stand for the m-dimensional hypervolume, or content, of body $\mathbf{B}_\alpha$. The Brünn–Minkowski theorem states that

$$R(\lambda) = \{V_m[\mathbf{B}(\lambda)]\}^{1/m} \tag{91}$$

is a concave function of λ in $0 \leqslant \lambda \leqslant 1$. In other words,

$$\{V_m[(1 - \lambda)\mathbf{B}_1 + \lambda\mathbf{B}_2]\}^{1/m} \geqslant (1 - \lambda)\{V_m[\mathbf{B}_1]\}^{1/m} + \lambda\{V_m[\mathbf{B}_2]\}^{1/m} \tag{92}$$

We refer the interested reader to Reference 29 for a proof of the theorem.

For present purposes $\mathbf{B}_1$ and $\mathbf{B}_2$ will be two parallel cross sections in polytope $P_N^{(\nu)}$. Thus (aside from a trivial translation dependent upon selection of an origin), the set of bodies $\mathbf{B}(\lambda)$ will be generated by connecting any point in $\mathbf{B}_1$ to any point in $\mathbf{B}_2$ by a straight line, and then forming the locus of points that cut that line in the length ratio λ: $(1 - \lambda)$. Body $\mathbf{B}(\lambda)$ will then lie in a hyperplane parallel to $\mathbf{B}_1$ and $\mathbf{B}_2$. This method of construction is shown in Fig. 15.

The bodies $\mathbf{B}_1$, $\mathbf{B}_2$, and $\mathbf{B}(\lambda)$ are all $[\nu(N - 1) - 1]$-dimensional entities, and so we take

$$m = \nu(N - 1) - 1 \tag{93}$$

in the basic inequality (92).[4] Because $P_N^{(\nu)}$ is convex, $\mathbf{B}(\lambda)$ lies entirely within the cross section $\mathbf{C}(\lambda)$ that its hyperplane forms with $P_N^{(\nu)}$ (see Fig. 15). Therefore we have

$$V_m[\mathbf{C}(\lambda)] \geqslant V_m[\mathbf{B}(\lambda)] \tag{94}$$

In conjunction with the Brünn–Minkowski theorem (92), this last result implies

$$\{V_m[\mathbf{C}(\lambda)]\}^{1/m} \geqslant (1 - \lambda)\{V_m[\mathbf{B}_1]\}^{1/m} + \lambda\{V_m[\mathbf{B}_2]\}^{1/m} \tag{95}$$

Since initial choice of parallel polytope cross sections $\mathbf{B}_1$ and $\mathbf{B}_2$ was arbitrary, we see that the $[\nu(N - 1) - 1]$-root of the content of a parallel family of polytope cross sections is always a concave function of displacement.

[4] For convenience we may think of $\mathbf{B}_1$, $\mathbf{B}_2$, and $\mathbf{B}(\lambda)$ as all projected into the same hyperplane parallel to each of them.

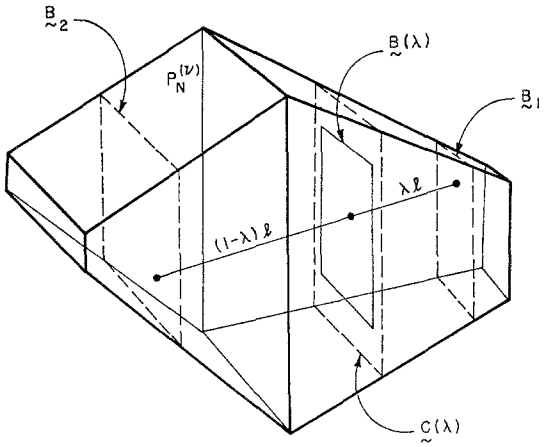

Fig. 15. Application of the Brünn–Minkowski inequality to parallel cross sections of polytope $P_N^{(\nu)}$. $\mathbf{B}(\lambda)$ in Eq. (89) is the locus of all points which divide straight-line connectors of sections $\mathbf{B}_1$ and $\mathbf{B}_2$ in the ratio $\lambda : (1 - \lambda)$. For $\lambda = 0,1$ the body $\mathbf{B}(\lambda)$ is coincident with $\mathbf{B}_1$, $\mathbf{B}_2$ respectively. $\mathbf{B}(\lambda)$ is always contained in $\mathbf{C}(\lambda)$, the cross section at position λ.

Section 3.1 demonstrated the proportionality between the various pair correlation contributions $g_{\nu n}(x)$ and associated cross section contents $C_{\nu n}(x)$. A useful test for the ergodicity of computer simulations (Monte Carlo or molecular dynamics) of rigid-particle systems under high compression is that each quantity

$$[g_{\nu n}(x)]^{1/[\nu(N-1)-1]} \tag{96}$$

should be a concave function of displacement x. Of course these are only necessary conditions, and are not sufficient to prove ergodicity.

So far as pair correlation in the large-system limit is concerned, the $g_{\nu n}$ themselves are of interest rather than the high-order roots shown in (96). Since the property of concavity is not generally preserved upon taking powers greater than 1, we cannot assert that the $g_{\nu n}(x)$ are concave. However, the absence of relative minima in any concave function *is* so preserved, and therefore each component function $g_{\nu n}(x)$ of $g^{(2)}(x)$ will be free of relative minima.

The conditions under which the $g_{\nu n}(x)$ are free of relative minima (i.e., are just single peaks) can be extended beyond perfect crystals. We have already noted that the presence of immobile vacancies and (in three dimensions) certain dislocations such as stacking faults again leads to a convex limiting polytope, although with reduced symmetry. Even with this broad class of imperfect crystals the Brünn–Minkowski theorem applies, and the individual pair-correlation components $g_{\nu n}(x)$ are all free of relative minima, regardless of the number and arrangement of defects.[5]

[5] In the perfect-crystal considerations in Section 3.1, it sufficed to consider an angle-average pair correlation function. With defects present it is desirable and possible to generalize the polytope cross section representation of pair correlation to individual particle pairs. These pairs can have a large number of arrangements relative to a defect, but for each the nonexistence of relative minima applies.

Our considerations also admit of a generalization to higher-order correlation functions. Let us first consider the case of triplets (ijk), and

$$Kg^{(3)}_{ijk}(x_{ij}, x_{jk}) \tag{97}$$

will stand for the probability that the pairs (ij) and (jk) are simultaneously separated by the regular lattice spacings plus x_{ij} and x_{jk} respectively (positive constant K is irrelevant for present purposes). The triplet probabilities already encountered in the Born–Green–Yvon equation analysis are special cases of these quantities (97), but it is easy to see that the entire class of such triplet functions may be identified with the $[\nu(N-1)-2]$-dimensional intersection of the two polytope cross sections belonging to pairs (ij) and (jk).

Suppose that the two relative displacements x_{ij} and x_{jk} in (97) vary in such a way that a linear parametric representation in terms of variable s obtained:

$$\begin{aligned} x_{ij}(s) &= \alpha_{ij} + \beta_{ij}s \\ x_{jk}(s) &= \alpha_{jk} + \beta_{jk}s \end{aligned} \tag{98}$$

where the α's and β's are constants. Then as s varies, the two cross sections move so that their intersection E_{ijk} sweeps out a third cross section.[6] This behavior is illustrated in Fig. 16, once again in three-dimensional version. This new cross section is of course a convex $[\nu(N-1)-1]$-dimensional polytope, and the family of intersections E_{ijk} is precisely a family of parallel cross sections in this *new* polytope. Therefore along any path of form (98), the set of triplet probabilities (97) will exhibit no relative minima.

Bent triplets (ijk) are open to specification by three simultaneous relative displacements, rather than just the two appearing as arguments of the triplet probabilities (97). This more specific set of probabilities might be denoted thus;

$$\bar{K}\bar{g}^{(3)}_{ijk}(x_{ij}, x_{jk}, x_{ik}) \tag{99}$$

and each would be proportional to the $[\nu(N-1)-3]$-dimensional mutual intersection $\bar{E}_{ijk}$ formed by the three hyperplanes through $P_N^{(\nu)}$ that correspond to the pair distances x_{ij}, x_{jk}, and x_{ik}. If these distances are constrained to follow a linear parametrization

$$\begin{aligned} x_{ij} &= \alpha_{ij} + \beta_{ij}s \\ x_{ik} &= \alpha_{ik} + \beta_{ik}s \\ x_{jk} &= \alpha_{jk} + \beta_{jk}s \end{aligned} \tag{100}$$

then as s varies, $\bar{E}_{ijk}$ sweeps out a convex $[\nu(N-1)-2]$-dimensional polytope by parallel displacement. We conclude that triplet functions (99) can have no relative minima along any path of type (100).

In the case of an arbitrary n-tuple of particles, probabilities can be defined which specify the simultaneous occurrence of a number of relative pair displacements

[6] The hypersurface so swept out will be flat *only* if x_{ij} and x_{jk} are linearly related, as in (98).

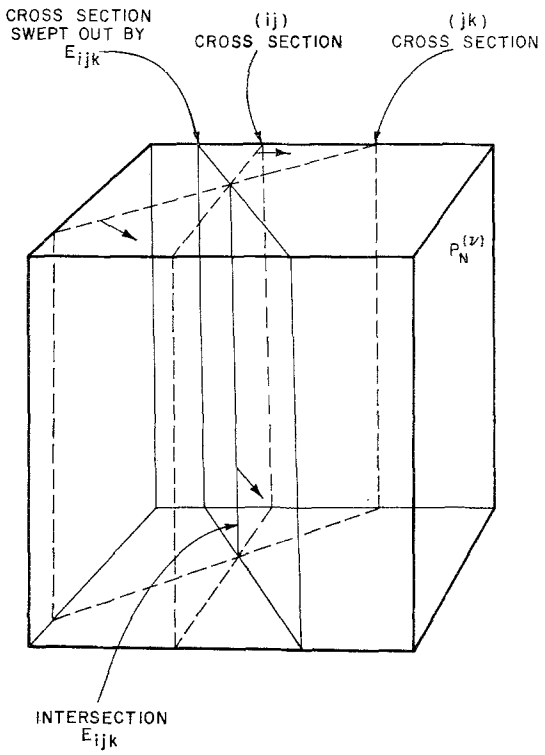

Fig. 16. Cross section swept out by the intersection of two other cross sections. The positions of the latter are linearly related [Eq. (98)].

anywhere from the greatest integer in $\frac{1}{2}(n+1)$, up to a maximum of $(\nu/2)(2n-\nu-1)$ if $n > \nu$. If all of these pair distances are linearly parameterized,

$$x_\mu(s) = \alpha_\mu + \beta_\mu s \tag{101}$$

(μ is a running index for the requisite number of distances), the nth-order probability along path (101) will be free of relative minima. This feature, furthermore, is valid regardless of the presence of immobile crystal defects.

6. GENERALIZED EULER THEOREM[7]

One of the landmarks of modern geometry was Euler's discovery in 1752 of a general linear relation between the number of faces (f), edges (e), and vertices (v) for any convex polyhedron in three dimensions:

$$f - e + v = 2 \tag{102}$$

[7] The reader is referred to Chapter 8 in Reference 6 for historical background and a proof of this theorem.

It was recognized by Schäfli a century later that a simple generalization of the Euler theorem could be formulated to describe convex polytopes in Euclidean spaces of arbitrary dimensionality. We now turn attention to the interpretation and application of this generalized Euler theorem to limiting polytopes $P_N^{(\nu)}$.

A general D-dimensional polytope $\mathscr{P}_D$ will be characterized by a set of numbers $f_k(\mathscr{P}_D)$, where $0 \leqslant k \leqslant D-1$, giving the number of "$k$-faces." This set of numbers is the generalization of the $D = 3$ triplet f, v, e:

$$f_2(\mathscr{P}_3) = f, \qquad f_1(\mathscr{P}_3) = e, \qquad f_0(\mathscr{P}_3) = v \tag{103}$$

but in the more general circumstance f_k is a count of the number of constituent k-dimensional subpolytopes. In terms of these numbers, the generalized Euler theorem states

$$\sum_{k=0}^{D-1} (-1)^k f_k(\mathscr{P}_D) = 1 - (-1)^D \tag{104}$$

for any convex polytope $\mathscr{P}_D$. Equation (102) is clearly a special case. Although (104) constitutes a necessary condition that a D-tuple of nonnegative integers $\{f_k\}$ describe an actual polytope, it is not sufficient—in fact no general criterion is presently available to decide which D-tuples satisfying the Euler relation belong to polytopes.

The enumeration of k-faces for rigid-particle limiting polytopes is straightforward in principle. The k-faces of maximal dimensionality $D-1$ [or $\nu(N-1)-1$, in the previous notation] are precisely the faces corresponding to the restraint of contact between nearest-neighbor pairs. Therefore f_{D-1} will exactly equal the number of nearest-neighbor pairs in the system:

$$f_{D-1} = \tfrac{1}{2} z_{\nu 1} N \tag{105}$$

Similarly, f_{D-2} enumerates the ways in which two pairs of nearest neighbors may simultaneously be in contact, so that

$$f_{D-2} = (1/2!)[\tfrac{1}{2} z_{\nu 1} N][\tfrac{1}{2} z_{\nu 1} N - 1] \tag{106}$$

except in the case of such trivially small systems that periodicity prevents the simultaneous contacts ($N = 1, 2$).

Complete enumeration of the k-faces is elementary for rigid rods, owing basically to the fact that the polytope is a simplex. Reference to Fig. 3 shows that with N rods, any collection of $N-1$ or fewer neighbor pairs may simultaneously be in contact. Under the restraint of j such contacts, the number of degrees of freedom of the system has been reduced by j, so that the relevant face is a $(D-j)$-face. Elementary combinatories gives ($D = N - 1$)

$$f_k(N \text{ rods}) = \frac{N!}{(N-k-1)!\,(k+1)!} \tag{107}$$

Except for the transposition of terms, this last result shows that the generalized Euler theorem for rigid rods is merely the statement

$$(1-1)^{D+1} = 0 \tag{108}$$

in binomial expansion form.

The content of the generalized Euler theorem, however, is far less obvious in the case of rigid disks and spheres. In these $\nu > 1$ systems, the f_k for $k = D - 1, D - 2,\ldots, D - 5$ start off obeying the simple combinatorial formula (107) expected for independent contacts, as (105) and (106) illustrate. However, this scheme goes awry at $k = D - 6$ because of a phenomenon without precedent in rigid rods, that is illustrated in Fig. 17. If one demands the six contacts around a hexagon of particles surrounding a seventh, the entire septuplet experiences a cooperative "jamming" effect that reduces the number of degrees of freedom not by six, but by eleven! As Fig. 17 also shows, precisely this same jamming would have occurred if the six contacts chosen formed a starlike pattern radiating outward from a central particle to six neighbors in a plane. Hence f_{11} is augmented at the expense of f_6.

In assessing the number of degrees of freedom available to a cluster of particles subject to a set of enforced contacts, it is useful to recognize that our high-compression limit renders disks equivalent to oriented rigid hexagons (due to the negligible effect

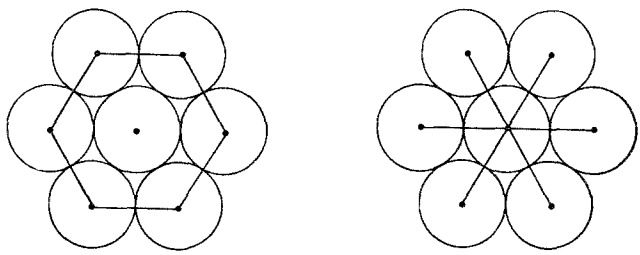

(a) EQUIVALENT "JAMMED" SEPTUPLETS

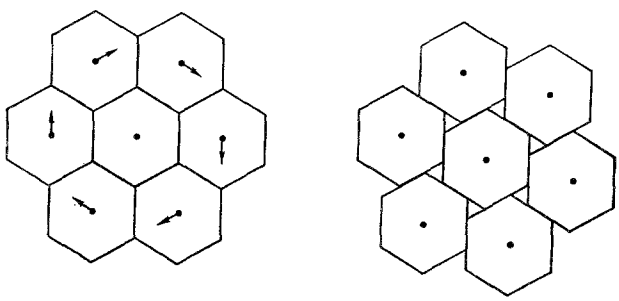

(b) SEPTUPLET ROTATION

Fig. 17. Cooperative "jamming" of particle clusters. In (a), forcing six contacts in either of the two ways shown (as solid lines between centers) causes a loss of eleven degrees of freedom. Beside translation, the septuplet may rotate as in (b), where particles are shown as their equivalent oriented flat-sided bodies.

of curvature), and spheres to oriented dodecahedra. Figure 17(b) illustrates the rotational freedom still available to seven jammed disks, as a cooperative sliding motion of the oriented hexagons. On account of the very small motion amplitudes available at high compression, it is consistent to regard the distance between hexagon centers unchanged during the sliding.

It is clear that the jamming phenomenon will occur in a wide variety of contact-constraint sets. For rigid disks, Fig. 18 presents two more jammed situations (as well as one which careful analysis shows is *not* jammed). Rigid spheres present an even more varied collection of possibilities, of course.

Sets of explicitly imposed contacts between nearest neighbors may always be put into correspondence with linear graphs on the lattice. Not only is the complete enumeration of such graphs unsolved for $\nu > 1$, but there is still the general problem of deciding how many degrees of freedom a given graph removes (i.e., how much

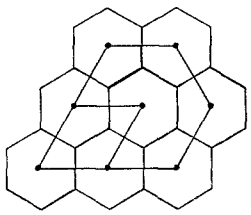

(a) UNJAMMED CLUSTER

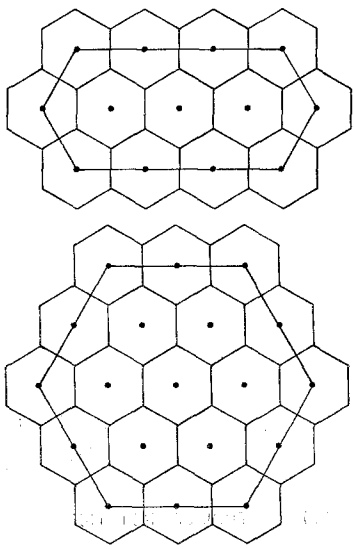

(b) JAMMED CLUSTERS

Fig. 18. Further examples of contact constraints in the rigid-disk system. The disks are represented by their equivalent oriented hexagons, and the required contacts indicated by lines between centers.

jamming it produces). As Fig. 17(a) demonstrates, graphs fall into equivalence classes; the Euler theorem then relates the numbers of those equivalence classes with a weight determined by number of lost degrees of freedom.

The existence of the jamming phenomenon has a direct bearing on the character of distance distribution functions for the particles involved. Let **G** be a graph connecting n particle centers, and let $p^{(n)}(x \mid \mathbf{G})$ stand for the probability that *all* bonds of **G** have length given by x (defined as the usual reduced distance, $x = -1$ giving contact). As x approaches -1 from above so that the n particles are put into contact as specified by **G**,

$$\lim_{x \to -1} p^{(n)}(x \mid \mathbf{G}) > 0 \tag{109}$$

if **G** involves no jamming. In other words, $p^{(n)}(x \mid \mathbf{G})$ behaves qualitatively in the same way as a product, or superposition, of pair-correlation functions for the separate links of **G**:

$$p^{(n)}(x \mid \mathbf{G}) \approx \text{const} \times [g_{\nu 1}(x)]^{l(\mathbf{G})} \qquad \text{(no jamming)} \tag{110}$$

[$l(\mathbf{G})$ is the number of links, or bonds, in **G**].

On the other hand, if **G** leads to jamming, the behavior is entirely different. As a result of the decreasing freedom of motion of particles as $x \to -1$, one finds instead

$$p^{(n)}(x \mid \mathbf{G}) \sim \text{const} \times (x + 1)^{d(\mathbf{G})} \qquad \text{(jamming)} \tag{111}$$

where $d(\mathbf{G})$ is the *extra* number of degrees of freedom lost above and beyond the $l(\mathbf{G})$ that "normally" obtain in an unjammed cluster [$d(\mathbf{G}) = 5$ for the examples in Fig. 17]. Thus the jamming phenomenon is associated with a gross violation of the superposition approximation for a graph's associated nth-order distribution function. Consistent with remarks in Section 3.1 one identifies the geometrical basis for this result with a change toward lower dimensionality of the k-face of $P_N^{(\nu)}$ at which the relevant sectioning hyperplane for the distribution function enters the polytope.

By actually enumerating all k-faces for some simple $P_N^{(\nu)}$, $\nu > 1$, we can quickly infer the fantastic geometrical complexity of limiting polytopes for even modest-size systems. The most elementary nontrivial case is two rigid disks, shows in Fig. 19(a). This system has polytope dimensionality

$$D = 2(2 - 1) = 2 \tag{112}$$

and four independent contact pairs (so that the polytope is merely a planar quadrilateral). One easily verifies that there are four possible pairs of pairs that may simultaneously be in contact; hence

$$\begin{aligned} f_1 &= 4 \\ f_0 &= 4 \end{aligned} \tag{113}$$

and the Euler relation reads

$$-4 + 4 = 1 - (-1)^2 \tag{114}$$

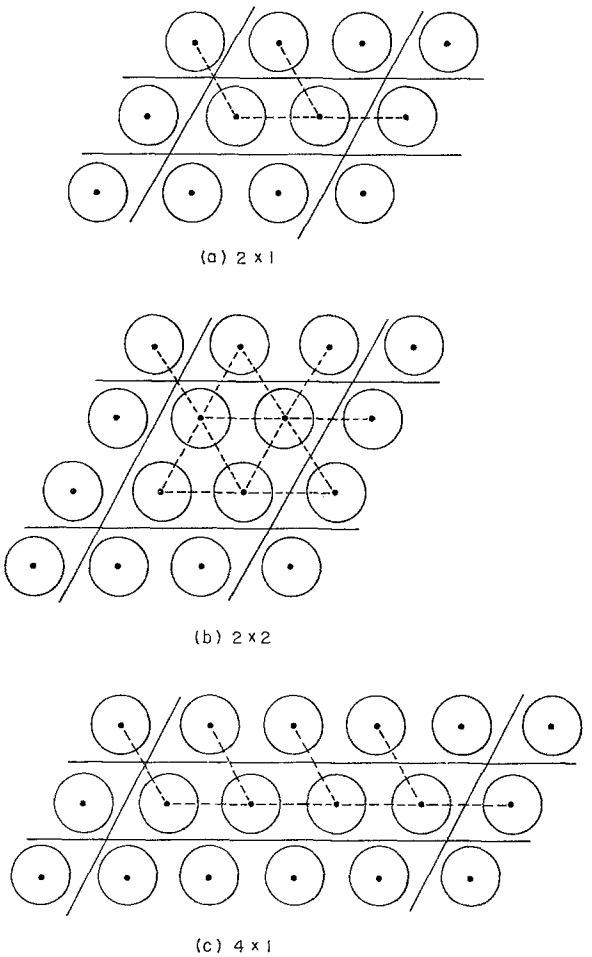

Fig. 19. Some small rigid disk systems (expanded for clarity) for which the k-face enumeration is carried out in the text. The dashed lines locate the independent pair contacts.

From the transparent 2×1 system, we pass on to examine the more interesting cases of 2×2 and 4×1 rigid-disk crystals, shown in Fig. 19(b) and (c). The polytope dimensionality D now is 6. Without too much difficulty one obtains the following:

$$\begin{array}{lrr} & \underline{2 \times 2} & \underline{4 \times 1} \\ f_5 = & 12 & 8 \\ f_4 = & 60 & 28 \\ f_3 = & 160 & 56 \\ f_2 = & 240 & 68 \\ f_1 = & 192 & 48 \\ f_0 = & 64 & 16 \end{array} \tag{115}$$

Not only do these results indicate an extremely rapid increase in polytope complexity as the number N of particles increases, but they also illustrate that a compact crystal (2×2) has more underlying geometrical structure than a long thin crystal (4×1) with the same number of particles. Doubtless this is due to the more "cooperative" (i.e., two-dimensional) nature of the former compared to the essentially linear latter.

Even by the time one considers the 3×3 rigid-disk crystal in a rhombic unit cell, the enumeration problem becomes very tedious. The first few k-face counts are found to be ($D = 16$)

$$\begin{aligned} f_{15} &= 27 \\ f_{14} &= 351 \\ f_{13} &= 2{,}916 \\ f_{12} &= 17{,}334 \\ f_{11} &= 78{,}246 \\ f_{10} &= 277{,}812 \end{aligned} \tag{116}$$

We invite the interested reader to extend the list, the missing members of which the Euler theorem states must satisfy

$$\sum_{k=0}^{9} (-1)^k f_k = -214{,}308 \tag{117}$$

7. POLYTOPE MOMENT TENSOR

Reduced displacement vectors $\mathbf{t}_i$, suitable for description of particle motions in the highly compressed crystals, were defined in Eq. (12). For notational simplicity, we now introduce the νN-component direct sum vector

$$\mathbf{t}^* = \mathbf{t}_1 \oplus \mathbf{t}_2 \oplus \cdots \oplus \mathbf{t}_N \tag{118}$$

which comprises the state of the entire system. The polytope moment tensor $\mathbf{T}$ is now defined as the canonical average of the dyad $\mathbf{t}^*\mathbf{t}^*$, under the restraint of fixed system center of mass:

$$\begin{aligned} \mathbf{T} = \langle \mathbf{t}^*\mathbf{t}^* \rangle &= \frac{\int d^{\nu N}\mathbf{t}^*(\mathbf{t}^*\mathbf{t}^*)\, \delta(\sum_{i=1}^{N} \mathbf{t}_i)}{\int d^{\nu N}\mathbf{t}^* \delta(\sum_{i=1}^{N} \mathbf{t}_i)} \\ &= [P_N^{(\nu)}]^{-1} \int_{P_N^{(\nu)}} d^{\nu(N-1)}\mathbf{t}^*(\mathbf{t}^*\mathbf{t}^*) \end{aligned} \tag{119}$$

One of the more interesting aspects of the limiting polytope theory is the relation between $\mathbf{T}$ and the crystal's elastic properties, as we shall presently establish.

The moment tensor $\mathbf{T}$ is equivalent to the inertia tensor $\mathbf{I}$ for $P_N^{(\nu)}$ if this polytope is regarded as a rigid body with uniform mass density and unit total mass.

In particular,

$$\mathbf{I} = (\mathrm{Tr}\ \mathbf{T})\mathbf{1} - \mathbf{T} \tag{120}$$

where $\mathbf{1}$ is the unit tensor. By taking the trace of both sides in this last equation, we have

$$\mathrm{Tr}\ \mathbf{T} = (\nu N - 1)^{-1}\ \mathrm{Tr}\ \mathbf{I} \tag{121}$$

which then permits Eq. (120) to be rewritten thus:

$$\mathbf{T} = (\nu N - 1)^{-1}\ (\mathrm{Tr}\ \mathbf{I})\mathbf{1} - \mathbf{I} \tag{122}$$

Therefore knowledge of either $\mathbf{T}$ or $\mathbf{I}$ allows us to find the other.

The eigenvalues of $\mathbf{I}$ are precisely the rotational moments of inertia of the homogeneous rigid body $P_N^{(\nu)}$ [as well as a single zero eigenvalue due to the fixed-center-of-mass constraint in (119)]. The form of Eq. (122) makes it clear that the same principal axes which diagonalize $\mathbf{I}$ also do the same for $\mathbf{T}$; in that rotated coordinate system the νN eigenvalues T_α of $\mathbf{T}$ are arranged along the diagonal, and are simply related to the corresponding polytope moments of inertia I_α :

$$T_\alpha = \left[(\nu N - 1)^{-1} \sum_{\gamma=1}^{\nu N} I_\gamma\right] - I_\alpha \tag{123}$$

If the rigid-particle crystal were contained by hard reflecting walls, the diagonalization of $\mathbf{T}$ would generally be very difficult. Our use of periodic boundary conditions, though, renders the diagonalization easy. As might well be expected with translational periodicity, one is obliged to introduce running-wave collective coordinates. Using $\mathbf{r}_j^{(0)}$ to denote undisplaced particle positions [as in Section 2.1], these collective coordinates may be written as follows in terms of reciprocal lattice vectors $\mathbf{k}$:[30]

$$\left.\begin{aligned} \boldsymbol{\chi}(0) &= N^{-1/2} \sum_{j=1}^{N} \mathbf{t}_j \\ \boldsymbol{\chi}(\mathbf{k}) &= (2/N)^{1/2} \sum_{j=1}^{N} \mathbf{t}_j \cos(\mathbf{k} \cdot \mathbf{r}_j^{(0)}) \\ \boldsymbol{\sigma}(\mathbf{k}) &= (2/N)^{1/2} \sum_{j=1}^{N} \mathbf{t}_j \sin(\mathbf{k} \cdot \mathbf{r}_j^{(0)}) \end{aligned}\right\} \quad \text{for } \mathbf{k} \neq 0 \tag{124}$$

By restricting the $\mathbf{k}$'s to one-half Brillouin zone, the N real vector collective coordinates $\boldsymbol{\chi}$ and $\boldsymbol{\sigma}$ will be independent; furthermore the transformation Jacobian from the $\mathbf{t}_j$ is unity.

The collective coordinate vector $\boldsymbol{\chi}(0)$ locates the crystal center of mass. Since our analysis of polytope geometry must be carried out under the restraint of fixed center of mass, we simply presume that $\boldsymbol{\chi}(0)$ has some suitable constant value and suppress its further consideration.

In order to show that the configuration space rotation (124) diagonalizes **T**, it is necessary to compute averages of the type

$$\begin{aligned}\langle \chi(\mathbf{k})\,\chi(\mathbf{k}')\rangle &= (2/N)\sum_{j,l=1}^{N}\cos(\mathbf{k}\cdot\mathbf{r}_j^{(0)})\cos(\mathbf{k}'\cdot\mathbf{r}_l^{(0)})\langle \mathbf{t}_j\mathbf{t}_l\rangle \\ &= (2/N)\sum_{j,l=1}^{N}\cos(\mathbf{k}\cdot\mathbf{r}_j^{(0)})[\cos(\mathbf{k}'\cdot\mathbf{r}_j^{(0)})\cos(\mathbf{k}'\cdot\mathbf{r}_{jl}^{(0)}) \\ &\quad - \sin(\mathbf{k}'\cdot\mathbf{r}_j^{(0)})\sin(\mathbf{k}'\cdot\mathbf{r}_{jl}^{(0)})]\langle \mathbf{t}_j\mathbf{t}_l\rangle \\ &= \delta_K(\mathbf{k}-\mathbf{k}')\sum_{l=1}^{N}\cos(\mathbf{k}\cdot\mathbf{r}_{1l}^{(0)})\langle \mathbf{t}_1\mathbf{t}_l\rangle \end{aligned} \tag{125}$$

In this expression, $\delta_K(\mathbf{q})$ is the vector Kronecker delta function

$$\begin{aligned}\delta_K(\mathbf{q}) &= 1, \qquad \mathbf{q} = 0 \\ &= 0, \qquad \mathbf{q} \neq 0\end{aligned} \tag{126}$$

By the same procedure, one also finds

$$\langle \sigma(\mathbf{k})\,\sigma(\mathbf{k}')\rangle = \delta_K(\mathbf{k}-\mathbf{k}')\sum_{l=1}^{N}\cos(\mathbf{k}\cdot\mathbf{r}_{1l}^{(0)})\langle \mathbf{t}_1\mathbf{t}_l\rangle \tag{127}$$

$$\langle \chi(\mathbf{k})\,\sigma(\mathbf{k}')\rangle = 0 \tag{128}$$

Thus **T** has no off-diagonal terms between different vector members of the χ, σ basis. For $\nu = 1$ this completes the diagonalization, but for $\nu > 1$, it still remains necessary to specify the ν-dimensional coordinate system which diagonalizes the dyadic sum common to expressions (125) and (127).

The rigid-disk crystal ($\nu = 2$) is sufficiently highly symmetrical that the dyadic sum will be diagonalized in a coordinate system with one axis parallel to "propagation vector" **k**, and the other axis perpendicular (transverse) to **k**. The independent disk crystal collective coordinates therefore may be interpreted as standing waves of pure longitudinal or transverse character. The situation will be quite analogous for the $\nu = 3$ face-centered cubic crystal, but with two degenerate transverse, and one longitudinal, mode for each **k**. The three-dimensional hexagonal close-packed crystal, however, has lower symmetry, and the collective modes will not generally be purely transverse and longitudinal in nature (except for special directions of **k**).

The fact that the collective coordinate transformation (124) is linear means that the condition that any single collective coordinate be constant, e.g.,

$$\chi_\alpha(\mathbf{k}) = \text{const} \tag{129}$$

corresponds to a flat hyperplane in the multidimensional polytope space. The probability density for this single coordinate,

$$p[\chi_\alpha(\mathbf{k})] \tag{130}$$

will then be proportional to the cross-sectional "area" created by intersection of that hyperplane with $P_N^{(v)}$, in exactly the same way that the pair correlation peaks are created [Section 3.1]. By virtue of the Brünn–Minkowski theorem [Section 5], it follows that $p[\chi_\alpha(\mathbf{k})]$ can have at most a single maximum. In the case of a very large crystal, it can be argued that since separate regions should contribute independently to $p[\chi_\alpha(\mathbf{k})]$, the central limit theorem [31] would demand that this probability function be Gaussian:

$$p[\chi_\alpha] = (2\pi T_\alpha)^{-1/2} \exp(-\chi_\alpha^2/2T_\alpha) \tag{131}$$

Here we have inserted the $\mathbf{T}$ eigenvalue corresponding to coordinate χ_α, since

$$\langle \chi_\alpha^2 \rangle = T_\alpha \tag{132}$$

Of course, an exactly similar set of relations applies to the σ_α variables.

The long-wavelength sinusoidal distortions of a large crystal described as a deviation of χ_α (or σ_α) from the mean value zero may equally well be regarded as a thermally excited elastic wave. For that reason we may relate the small-$\mathbf{k}$ eigenvalues T_α to the isothermal elastic constants for the crystal. This in turn implies a relation between elasticity and polytope moments of inertia via Eq. (123).

These elasticity relations are easy to exhibit for the rigid-disk crystal. In that system, a displacement field $\mathbf{u}(\mathbf{r})$, which does not alter the system area, causes the free energy to change isothermally by an amount[8]

$$\delta F_N\{\mathbf{u}\} = \frac{1}{\Omega} \int_\Omega d^2\mathbf{r}\{2\lambda_{\xi\eta\xi\eta}(u_{xx} + u_{yy})^2 + \lambda_{\xi\xi\eta\eta}[(u_{xx} - u_{yy})^2 + 4u_{xy}^2]\} \tag{133}$$

Here, the two independent elastic constants are denoted by $\lambda_{\xi\eta\xi\eta}$ and $\lambda_{\xi\xi\eta\eta}$, and the u_{ij} are the symmetric strain tensor components.[32] In the high-compression regime, it has been established[8] that

$$\begin{aligned} \lambda_{\xi\eta\xi\eta} &= \frac{Nk_BT}{2[(\Omega/\Omega_0) - 1]^2} \\ \lambda_{\xi\xi\eta\eta} &= \frac{bNk_BT}{[(\Omega/\Omega_0) - 1]^2} \end{aligned} \tag{134}$$

where b is a positive constant of order unity (known at present only approximately, by the cell-cluster technique).[8] The displacement field for a given collective coordinate may be inserted in (133) to give the corresponding free energy; then the Boltzmann factor

$$\exp\{-\beta\, \delta F_N\} \tag{135}$$

is required to agree in exponent with Gaussian form (131).

The set of reduced disk displacements

$$\mathbf{t}_j = (2/N)^{1/2}\, \chi_l \cos(\mathbf{k} \cdot \mathbf{r}_j^{(0)})(\mathbf{k}/k) \tag{136}$$

amounts to a longitudinal wave with collective coordinate amplitude χ_l, and the associated displacement field is

$$\mathbf{u}(\mathbf{r}) = \frac{a\chi_l}{(2N)^{1/2}}\left(\frac{\Omega}{\Omega_0} - 1\right)\cos(\mathbf{k}\cdot\mathbf{r})\left(\frac{\mathbf{k}}{k}\right) \tag{137}$$

If this last expression is utilized in (133) for δF_N, one eventually finds that the band of "longitudinal" eigenvalues (subscript l) for rigid disk tensor $\mathbf{T}$ has the following small-$\mathbf{k}$ behavior:

$$T_l(\mathbf{k}) \sim \frac{2}{a^2(1+b)k^2} \tag{138}$$

A similar calculation for "transverse" eigenvalues (subscript t) gives

$$T_t(\mathbf{k}) \sim \frac{1}{2a^2bk^2} \tag{139}$$

Reference 8 indicates that b should be roughly 0.5, so that for a given small k, the longitudinal eigenvalue should exceed its transverse counterpart.

The same sort of small-k eigenvalue calculation may be carried out in one dimension (one elastic constant—the linear compressibility) or in three dimensions (three elastic constants for f.c.c., six for h.c.p.). Although the precise numerical coefficients will differ from case to case, the inverse-square dependence on k is quite general irrespective of ν. This feature causes the Gaussians (131) to become very broad as $k \to 0$. The family of polytope cross sections for a small-k collective coordinate direction is therefore very "strung out," that is, the polytope is very long in these directions.

If one were able to compute the exact eigenvalue spectrum for crystals at all $\mathbf{k}$'s, a reversal of our argument would yield the entire nonlocal linear elastic response characteristics. This features should eventually prove valuable in understanding sound dispersion in anharmonic solids.

The inverse to collective coordinate transformation (124) is

$$\mathbf{t}_j = N^{-1/2}\boldsymbol{\chi}(0) + (2/N)^{1/2}\sum_{\mathbf{k}\neq 0}[\cos(\mathbf{k}\cdot\mathbf{r}_j^{(0)})\,\boldsymbol{\chi}(\mathbf{k}) - \sin(\mathbf{k}\cdot\mathbf{r}_j^{(0)})\,\boldsymbol{\sigma}(\mathbf{k})] \tag{140}$$

Under the usual restraint of fixed system center of mass [$\boldsymbol{\chi}(0) = 0$ for convenience], we may calculate the displacement correlations for high-compression crystals thus:

$$\begin{aligned}\langle \mathbf{t}_j\mathbf{t}_l\rangle &= \frac{2}{N}\sum_{\mathbf{k}\neq 0}[\cos(\mathbf{k}\cdot\mathbf{r}_j^{(0)})\cos(\mathbf{k}\cdot\mathbf{r}_l^{(0)})\langle\boldsymbol{\chi}(\mathbf{k})\,\boldsymbol{\chi}(\mathbf{k})\rangle \\ &\quad + \sin(\mathbf{k}\cdot\mathbf{r}_j^{(0)})\sin(\mathbf{k}\cdot\mathbf{r}_l^{(0)})\langle\boldsymbol{\sigma}(\mathbf{k})\,\boldsymbol{\sigma}(\mathbf{k})\rangle] \\ &= \frac{2}{N}\sum_{\mathbf{k}\neq 0}\cos(\mathbf{k}\cdot\mathbf{r}_{jl}^{(0)})\langle\boldsymbol{\chi}(\mathbf{k})\,\boldsymbol{\chi}(\mathbf{k})\rangle\end{aligned} \tag{141}$$

As a special case we may set $j = l$, to obtain the quadratic displacement tensor for a single particle,

$$\langle \mathbf{t}_j\mathbf{t}_j\rangle = \frac{2}{N}\sum_{\mathbf{k}\neq 0}\langle\boldsymbol{\chi}(\mathbf{k})\,\boldsymbol{\chi}(\mathbf{k})\rangle \tag{142}$$

the trace of which will give the Debye–Waller factor.[33]

As N goes to infinity in such a way that all crystal dimensions likewise increase, the $\mathbf{k}$ sums in (141) and (142) pass to integrals formally:

$$\frac{2}{N}\sum_{\mathbf{k}\neq\mathbf{0}} \to \frac{2}{\tau}\int d^{\nu}\mathbf{k} \tag{143}$$

where the integral should be carried out over one-half of the Brillouin zone τ. The inverse-square behavior of the eigenvalues, illustrated by (138) and (139), implies that the mean-square deviation of rods and disks diverges (in the large-crystal limit), but is finite for rigid spheres.

The *relative* mean squared displacement of two particles may be written

$$\begin{aligned}\langle(\mathbf{t}_j - \mathbf{t}_l)(\mathbf{t}_j - \mathbf{t}_l)\rangle &= \frac{4}{N}\sum_{k\neq 0}[1 - \cos(\mathbf{k}\cdot\mathbf{r}_{jl}^{(0)})]\langle\chi(\mathbf{k})\,\chi(\mathbf{k})\rangle \\ &\xrightarrow{n\to\infty} \frac{4}{\tau}\int d^{\nu}\mathbf{k}[1 - \cos(\mathbf{k}\cdot\mathbf{r}_{jl}^{(0)})]\langle\chi(\mathbf{k})\,\chi(\mathbf{k})\rangle \end{aligned} \tag{144}$$

In the case of rods and disks the integral is now convergent on account of the bracketed trigonometric factor going to zero at the origin. But it is easy to show that for large $r_{jl}^{(0)}$, the result from (144) will be asymptotically proportional to $r_{jl}^{(0)}$ for rods, and to $\ln r_{jl}^{(0)}$ for disks, though it remains bounded with $r_{jl}^{(0)}$ for spheres. This is the basis for the allegation[34] that no long-range order can exist as an infinite-system property for rods and disks. We have therefore established a further connection between polytope geometry and crystalline order through the moment tensor $\mathbf{T}$.

8. OPEN QUESTIONS

The elementary geometrical theory of limiting polytopes has now been outlined. We conclude this survey with a list of unsolved problems in this field. By presenting this list, we hope to capture the interest of scholars who by training are able to contribute to a deeper understanding of the fascinating geometrical basis of the venerable rigid rod, disk, and sphere models in statistical mechanics.

A. As already mentioned in the Introduction, the principal omission in the present high-compression theory is a proof of commutability for the limits $N \to \infty$ and $\Omega \to \Omega_0$. There seems to be no reason to doubt that intensive quantities (such as equation of state, and distribution function peak shapes) established as infinite-N limits of $P_N^{(\nu)}$ properties are indeed the correct properties for infinite systems, but a rigorous demonstration will likely demand considerable mathematical ingenuity and sophistication.

B. Section 2.4 exhibited a sequence of upper free energy bounds which converge to the exact free energy. Procedures for obtaining equally tight lower bounds are lacking at present. Although we have seen that circumscribed hyperspheres about the $P_N^{(\nu)}$ are useless in providing a finite lower bound on free energy per particle as $N \to \infty$, possibly the smallest circumscribed hyperellipsoid might succeed, owing to its ability to follow the polytope in the latter's "long" directions. Alternatively, one might be

able to bound $P_N^{(\nu)}$ from above by finding the content of the maximal polytope with the same number of faces and r_{in}.

C. Can the relative stability of the face-centered cubic and the hexagonal sphere crystals be established purely through geometrical polytope properties? Also, can the sign of the spontaneous hexagonal crystal distortion be similarly determined?

D. The conclusion that distribution function components have single maxima, which follows from the Brünn–Minkowski theorem, is a rather weak constraint. It is desirable to find more powerful conditions, possibly even bounds, from information available about the polytope geometry.

E. What are the diameter and minimum width of the $P_N^{(\nu)}$? In particular, do the directions of the former (as implied by the results of Section 7) coincide with collective coordinate axes of minimum positive wave-vector magnitude k?

F. It is easy to show that the cross-sectional "area" genereated by a hyperplane (moving by parallel displacement) through a D-dimensional polytope consists piecewise of polynomial portions of degree D or less in the displacement variable. By analogy with the Yang–Lee general grand partition function theory,[35] it seems attractive to examine the limiting distribution of polynomial zeros (in the complex plane for the displacement variable) as system size tends to infinity.

G. The fact that the number of k-faces, f_k, for the simplectic $P_N^{(1)}$ is merely a binomial coefficient [Eq. (107)] implies that as N becomes very large, f_k becomes essentially Gaussian for k near $N/2$. The maximum number of k-faces is then sharply attained at k equal to the nearest integer to $N/2$. Do similar results apply to the rigid disk and sphere f_k? Is it possible that an appropriate distribution of crystal vacancies (e.g., all in one half of the crystal) could render f_k bimodal?

H. Although we have indicated that the eigenvalues of moment tensor $\mathbf{T}$ vary as k^{-2} for small wave vectors $\mathbf{k}$, it still remains an open question as to how one could calculate the details of the entire spectrum, even for the simple rigid rod system. The strong analogy between the phonons in harmonic crystals and the eigenfunctions of $\mathbf{T}$ suggests that the Brillouin zone boundaries should be extremal points for the various bands of $\mathbf{T}$ eigenvalues; one may in fact eventually be able to develop a theory of the van Hove type[36] for the singularities in the eigenvalue density.

I. How do isolated vacancies affect the eigenvalues and eigenfunctions of $\mathbf{T}$? Can a group of one or more vacancies have associated with it a "localized mode" analogous to those in harmonic lattices with light defect particles?[37]

J. What is the nature of the eigenfunctions of the tetradic displacement tensor $\langle \mathbf{t}^*\mathbf{t}^*\mathbf{t}^*\mathbf{t}^* \rangle$? Do they describe the mutual scattering of pairs of displacement waves?

K. What are the topological properties of the linear graphs formed by the 1-faces of limiting polytopes? In particular, do they possess Hamiltonian circuits (each vertex visited once and only once)?

L. Can the "cell-cluster" expansion for polytope content[10] be proved to converge (in the $N \to \infty$ limit) for $\nu > 1$?

ACKNOWLEDGMENTS

The authors wish to thank Dr. William W. Wood for providing the information shown in Fig. 8. They are also indebted to Dr. E. N. Gilbert for indicating the location of relevant mathematical theory for Section 5.

REFERENCES

1. H. L. Frisch, in: *Advances in Chemical Physics*, I. Prigogine, ed., Interscience Publishers, New York (1964), Vol. VI, p. 229.
2. J. D. Eshelby, in: *Solid State Physics*, F. Seitz and D. Turnbull, eds., Academic Press, Inc., New York (1965), Vol. 3, p. 79.
3. B. J. Alder, W. G. Hoover, and D. A. Young, *J. Chem. Phys.* **49**:3688 (1968).
4. W. W. Wood, Los Alamos Scientific Laboratory (Los Alamos, N. M.) Report LA-2827, "Monte Carlo Calculations of the Equation of State of Systems of 12 and 48 Hard Circles," 1963. (Available from Office of Technical Services, U.S. Dept. of Commerce, Washington, D.C.)
5. Z. W. Salsburg and W. W. Wood, *J. Chem. Phys.* **37**:798 (1962).
6. B. Grünbaum, *Convex Polytopes*, Interscience Publishers, New York (1967).
7. M. G. Kendall, *A Course in the Geometry of n Dimensions*, Hafner Publishing Co., New York (1961), p. 9.
8. F. H. Stillinger, Jr., and Z. W. Salsburg, *J. Chem. Phys.* **46**:3962 (1967).
9. A. D. Wyner, *Bell System Tech. J.* **44**:1061 (1965).
10. F. H. Stillinger, Jr., Z. W. Salsburg, and R. L. Kornegay, *J. Chem. Phys.* **43**:932 (1965).
11. Z. W. Salsburg, W. G. Rudd, and F. H. Stillinger, Jr., *J. Chem. Phys.* **47**:4534 (1967).
12. W. G. Rudd, Z. W. Salsburg, A. P. Yu, and F. H. Stillinger, Jr., *J. Chem. Phys.* **49**:4857 (1968).
13. L. Tonks, *Phys. Rev.* **50**:955 (1936).
14. E. Helfand, H. L. Frisch, and J. L. Lebowitz, *J. Chem. Phys.* **34**:1037 (1960).
15. W. G. Hoover and F. H. Ree, *J. Chem. Phys.* **49**:3609 (1968).
16. M. G. Kendall, *op. cit.*, p. 35.
17. Z. W. Salsburg, *J. Chem. Phys.* **44**:3752 (1966).
18. J. A. Barker, *Australian J. Phys.* **17**:259 (1964).
19. W. G. Rudd, *J. Chem. Phys.* **48**:619 (1968).
20. Z. W. Salsburg, R. W. Zwanzig, and J. G. Kirkwood, *J. Chem. Phys.* **21**:1098 (1953).
21. T. L. Hill, *Statistical Mechanics*, McGraw-Hill Book Company, Inc., New York (1956), p. 204.
22. N. Metropolis, A. W. Rosenbluth, M. N. Rosenbluth, A. H. Teller, and E. Teller, *J. Chem. Phys.* **21**:1087 (1953).
23. A. Rotenberg, "Monte Carlo Studies of Systems of Hard Spheres," Courant Institute of Mathematical Sciences, New York University, New York, N. Y., Rept. NYO-1480-3.
24. R. D. Larsen and Z. W. Salsburg, *J. Chem. Phys.* **45**:4190 (1966).
25. R. D. Larsen and Z. W. Salsburg, *J. Chem. Phys.* **47**:3334 (1967).
26. C. A. Rogers, *Packing and Covering*, Cambridge University Press, Cambridge (1964), pp. 14–15.
27. *Ibid.*, p. 3.
28. *Convexity*, V. L. Klee, ed., Proceedings of Symposia in Pure Mathematics, Vol. VII, American Mathematical Society, Providence, R. I. (1963).
29. H. G. Eggleston, *Convexity*, No. 47 of Cambridge Tracts in Mathematics and Mathematical Physics, Cambridge University Press, Cambridge (1958), p. 97.
30. L. Brillouin, *Wave Propagation in Periodic Structures*, Dover Publications, Inc., New York (1953), Chapters VI and VII.
31. W. Feller, *An Introduction to Probability Theory and Its Applications*, John Wiley and Sons, Inc., New York (1966), Vol. II, p. 252.
32. L. D. Landau and E. M. Lifshitz, *Theory of Elasticity* (translated by J. B. Sykes and W. H. Reid), Addison-Wesley Publ. Co., Reading, Mass. (1959), p. 2.
33. C. Kittel, *Quantum Theory of Solids*, John Wiley and Sons, Inc., New York (1963), p. 379.

34. F. H. Stillinger, Jr., E. A. DiMarzio, and R. L. Kornegay, *J. Chem. Phys.* **40**:1564 (1964).
35. C. N. Yang and T. D. Lee, *Phys. Rev.* **87**:404, 410 (1952).
36. A. A. Maradudin, E. W. Montroll, and G. H. Weiss, *Theory of Lattice Dynamics in the Harmonic Approximation*, Academic Press, New York (1963), pp. 76–84.
37. *Ibid.*, pp. 159–178.